Design Method of Adaptive Full Order Observer With or Without Estimated Flux Error in Speed Estimation Algorithm

Wei Sun, Yong Yu, Gaolin Wang, *Member, IEEE*, Binbin Li, and Dianguo Xu, *Senior Member, IEEE*

***Abstract*—The performance of adaptive full order observer for sensorless induction motor drives can be improved further though it has been researched for many years. In this paper, two different design methods for improving the speed estimation stability and robustness are proposed: 1) In classical speed estimation algorithm used in adaptive full order observer, the estimated rotor flux error is neglected. A robust design method of feedback gains with classical speed estimation algorithm is proposed. Compared with existed three main design methods of feedback gains, the stability of speed estimation and estimated speed error are improved. 2) A robust speed estimation algorithm with estimated rotor flux error and the corresponding feedback gains are proposed in this paper. Through Lyapunov's theorem, the stability of proposed speed estimation algorithm is proved. The stability of flux estimation and estimated speed error can be improved much more. Finally, the feasibility of two proposed methods is verified by experiments.**

***Index Terms*—Adaptive full order observer, induction motor, motor parameter deviation, speed estimation algorithm, speed sensorless.**

NOMENCLATURE

R_s	Stator resistance.
R_r	Rotor resistance.
L_s	Stator inductance.
L_r	Rotor inductance.
L_m	Mutual inductance.
ω_e	Rotor flux speed.
ω_r	Rotor speed.
ω_s	Slip speed.
λ_s	Stator flux.
λ_r	Rotor flux.
i_s	Stator current.
T_L	Load torque.
p	Differential operator.
$\rightarrow$	Denotes space vector quantities.
$\hat{}$	Denotes estimated values.
$*$	Denotes commanded values.
$[]_\alpha, []_\beta$	Suffixes denoting quantities on stationary reference frame.
$[]_d, []_q$	Suffixes denoting quantities on rotary reference frame.
$\boldsymbol{I}, \boldsymbol{J}, \boldsymbol{B}_v$	$= \begin{bmatrix} 1 & 0 \\ 0 & 1 \end{bmatrix}, = \begin{bmatrix} 0 & 1 \\ -1 & 0 \end{bmatrix}, = \begin{bmatrix} b_1 & 0 \\ 0 & b_1 \end{bmatrix}$.
$\boldsymbol{H_1}, \boldsymbol{H_2}$	$= \begin{bmatrix} h_1 & 0 \\ 0 & h_1 \end{bmatrix}, = \begin{bmatrix} h_2 & 0 \\ 0 & h_2 \end{bmatrix}$.
$\boldsymbol{G_1}, \boldsymbol{G_2}$	$= \begin{bmatrix} g_1 & g_2 \\ -g_2 & g_1 \end{bmatrix}, = \begin{bmatrix} g_3 & g_4 \\ -g_4 & g_3 \end{bmatrix}$, Observer's feedback gain.

Manuscript received November 6, 2014; revised March 29, 2015; accepted May 25, 2015. Date of publication June 4, 2015; date of current version November 16, 2015. This work was supported by the Research Fund for the National Science Foundation of China under Grant 51207030. Recommended for publication by Associate Editor R. Kennel.

The authors are with the School of Electrical Engineering and Automation, Harbin Institute of Technology, Harbin 150001, China (e-mail: sunwei198677@hotmail.com; yuyong@hit.edu.cn; wgl818@hit.edu.cn; libinbinhit@126.com; xudiang@hit.edu.cn).

Color versions of one or more of the figures in this paper are available online at http://ieeexplore.ieee.org.

Digital Object Identifier 10.1109/TPEL.2015.2440373

I. INTRODUCTION

In application speed sensor is expensive and unreliable in hostile environments. It is necessary to use speed sensorless drives instead. In general, the advantages of speed sensorless drives include low cost, reduced hardware complexity and size, improved reliability and less maintenance requirements [1]. The main disadvantage of speed sensorless drives is the poor performance when induction motor runs at low speed range or at zero speed point. However, the low-speed and zero speed operating situation of induction motor in industry applications is common, such as hoist (operating at 0.5 to 1 Hz sometimes), carrier car used for transport in mine (operating at 0 Hz sometimes) and cutting machine for marble (operating at 0.3 Hz sometimes). So it is needed to improve the performance of speed sensorless drives at low speed range whatever in the motoring mode or in the regenerating mode.

Many approaches of speed sensorless induction motor drives have been proposed in past years. There are mainly two basic approaches in sensorless control system. One approach is based on fundamental model of induction motor. Fundamental model has poor performance when motor runs at low speed range in motoring mode or in regenerating mode. The other approach is signal-injection-based method for speed estimation, which is based on rotor slot harmonics, main inductance saturation, artificial saliency or rotor slot leakage. With signal injection, the motor can run at zero speed.

In signal-injection-based observer, a spatial salience in motor is assumed. It is difficult to extract right information, and the salience of motor varies in different motors. Because of the poor universality, the signal-injection-based method is not often used in practical application. Instead of signal injection the fundamental-model-based methods are used more often. With

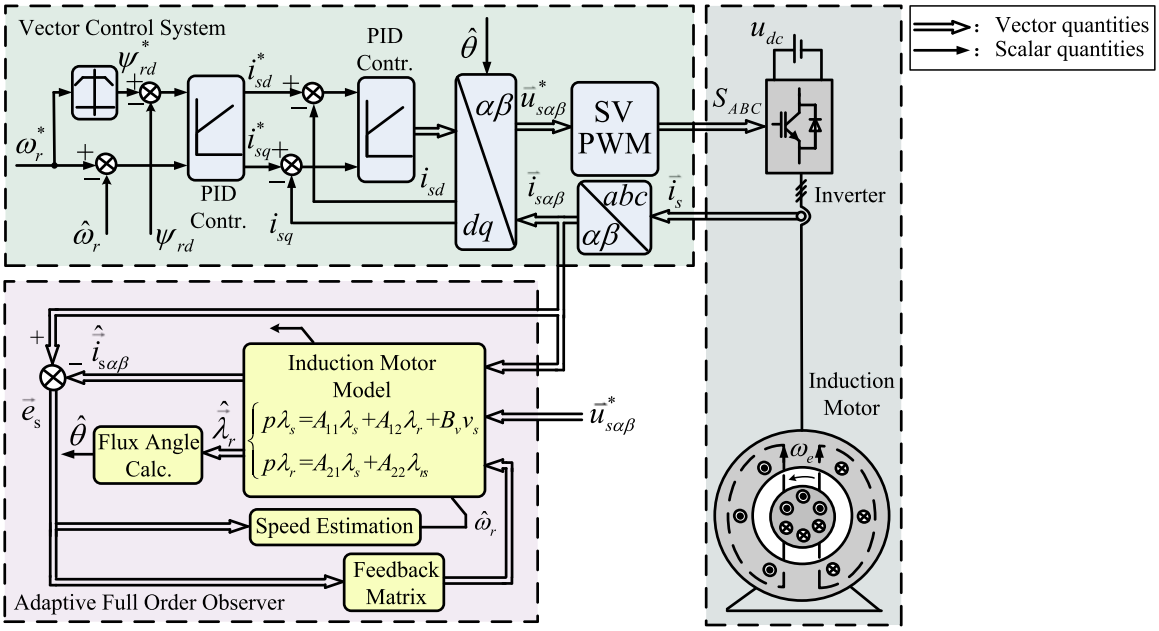

Fig. 1. Structure of adaptive full order observer for speed sensorless induction motor drives.

this method an observer for flux and rotor speed estimation is established using fundamental model of induction motor. About the observer, there are mainly three methods being well researched: field orientation control (FOC) [2]–[8], direct torque control (DTC) [9]–[11], and predictive torque control (PTC) [12], [13].

The performance of DTC method is similar to the FOC method, but compared with FOC, DTC is not used widely. PTC is the method which combines DTC with predictive control. It is the newest method in recent years and there are few applications in industry. FOC method is a mature speed sensorless control method that has been well researched in decades. It includes open-loop observer [2], model reference adaptive system (MRAS) [3]–[6], adaptive full-order and reduced-order [14] observer, and Kalman filter observer [15]. In [16], MRAS and voltage current observer are combined for rotor flux and speed estimation. Especially, the signal injection is used for online rotor time constant tuning.

In [17], three different flux observers are compared on parameter sensitivity, load torque impact and system stability. It can be concluded that adaptive full order observer has better performance when motor parameter deviates, and has larger stable region than other two observers. In decades many works for adaptive full order observer (AFO) have already been done. In [18]–[20], feedback gain matrix of observer is designed through observer's pole placement. In [21], through design of gain matrix, the estimated rotor flux error can be reduced especially in low-speed range. In [22], gain matrix is designed for stability in low-speed regenerating mode. In [23], AFO is combined with signal injection for better low-speed performance. In [24], state observability of AFO is analyzed in detail. In [25], feedback gain matrix is designed for stability improvement in permanent magnet synchronous motor drives and experiment results show well performance especially at zero speed. In [26], AFO and reduced-order observer are compared on stability with uncertain parameters. Compared with AFO, there are other effective methods combining adaptive adjustment for performance improving in sensorless induction motor drives. In the literature [33], the method of online parameter identification is proposed. In this method, the estimated motor parameters can always equal the actual motor parameters during long time operation. The system robustness is improved. But there is unstable area for motor parameters estimation at low speed range. In the literature [34], the robust Kalman filter and adaptive speed estimation are proposed. Although the sensitivity to external and internal interrupt is decreased at middle and high speed range, the performance at low speed range is not well. In the literature [16], a signal is injected for motor parameter identification. This method can identify the motor parameters at all speed range. The accuracy of identification can also be guaranteed. But the signal injection can cause the fluctuation of torque.

In recent years there are few literatures about the AFO method for speed sensorless induction motor drives. However, the performance of AFO can be improved further. In this paper, only AFO without any combination like signal injection or online parameters identification is researched. Fig. 1 indicates the structure of AFO and direct rotor FOC which is used in this paper. To improve the performance of AFO further, two different robust design methods for AFO are proposed.

Table I indicates the comparison between existed three main design methods and two proposed design methods for AFO. In existed methods, only design method for feedback gains is discussed and the classical speed estimation, in which estimated rotor flux error is neglected, is used.

A: based on poles placement of observer. Its purpose is to make convergence rate of observer faster than motor.

TABLE I
COMPARISON BETWEEN CLASSICAL AND PROPOSED METHOD

	Method	Flux Error in Speed Estimation	Performance
Classical Method	A	no	Advantage: convergence rate of observer is faster than motor Disadvantage: instability of speed estimation in low-speed regenerating mode
	B	no	Advantage: making minimum error of estimated rotor flux Disadvantage: instability of speed estimation in low-speed regenerating mode
	C	no	Advantage: guaranteeing stability of speed estimation at all speed range Disadvantage: large estimated speed error due to parameter deviation
Proposed Method	D	no	Advantage: guaranteeing stability of speed estimation at all speed range and smaller estimated speed error due to parameter deviation Disadvantage: convergence rate of observer is smaller than motor
	E	yes	Advantage: guaranteeing stability of speed estimation at all speed range and almost no estimated speed error due to parameter deviation and improved stability in digital system Disadvantage: complicated design process

B: based on estimated rotor flux error. Its purpose is to obtain minimum error of estimated rotor flux.

C: based on stability of estimated speed when induction motor runs in regenerating mode. Its purpose is to make speed estimation stable at all speed range.

D: based on stability of estimated speed when induction motor runs in regenerating mode. This method, as the improvement of method C, has the same purpose as method C. But the design process of feedback gains is different. The designed feedback gains are also different.

E: based on a speed estimation algorithm considering estimated rotor flux and proposing the corresponding feedback gains. Its purpose is to improve the system stability and robustness to motor parameter deviation further.

The AFO design method without the flux error in the speed estimation has been researched many years. This type of design method includes three typical methods: the method A, B and C. But the performance of this type of design can still be improved. So the method D, as the improvement of method C, is proposed. With method D the estimated speed sensitivity to stator and rotor resistance is reduced especially the sensitivity to rotor resistance is reduced by half. The main contribution of the paper is introducing the flux error to the speed estimation and designing the corresponding feedback gains. This method can not only guarantee the stability of speed estimation in regenerating and motoring mode at same time, but also improve the robustness of speed estimation further. Its theoretical analysis is presented in Section IV and its feasibility is verified by experiments in Section V.

In this paper, Section II introduces the fundamental model of induction motor and adaptive full order observer. The performances of existed three main design methods for AFO are analyzed. Section III presents the design process of method D. It is the improvement of method C. The performances of two methods are indicated. Section IV indicates the robust speed estimation algorithm with estimated rotor flux error and the corresponding feedback gains. Finally, the comparison between existed methods and proposed methods are indicated.

II. CLASSICAL SPEED ESTIMATION AND CLASSICAL FEEDBACK GAINS

In rotary reference frame, the dynamic model of induction motor is given by (1)

$$\begin{cases} p\vec{\lambda}_s = \boldsymbol{A_{11}}\vec{\lambda}_s + \boldsymbol{A_{12}}\vec{\lambda}_r + \boldsymbol{B}_v\vec{v}_s \\ p\vec{\lambda}_r = \boldsymbol{A_{21}}\vec{\lambda}_s + \boldsymbol{A_{22}}\vec{\lambda}_r \\ \vec{i}_s = \boldsymbol{H_1}\vec{\lambda}_s + \boldsymbol{H_2}\vec{\lambda}_r \end{cases} \tag{1}$$

where

$$\begin{aligned} \vec{\lambda}_s &= \begin{bmatrix} \lambda_{sd} & \lambda_{sq} \end{bmatrix}^T, \vec{\lambda}_r = \begin{bmatrix} \lambda_{rd} & \lambda_{rq} \end{bmatrix}^T \\ \vec{v}_s &= \begin{bmatrix} v_{sd} & v_{sq} \end{bmatrix}^T, \vec{i}_s = \begin{bmatrix} i_{sd} & i_{sq} \end{bmatrix}^T \\ \boldsymbol{A_{11}} &= a_{11}\boldsymbol{I} + \omega_e\boldsymbol{J}, \boldsymbol{A_{12}} = a_{12}\boldsymbol{I} \\ \boldsymbol{A_{21}} &= a_{21}\boldsymbol{I}, \boldsymbol{A_{22}} = a_{22}\boldsymbol{I} + (\omega_e - \omega_r)\boldsymbol{J} \\ a_{11} &= \frac{-R_s}{\delta L_s}, a_{12} = \frac{R_s L_m}{\delta L_s L_r}, a_{21} = \frac{R_r L_m}{\delta L_s L_r}, a_{22} = \frac{-R_r}{\delta L_r} \\ b_1 &= 1, h_1 = \frac{1}{\delta L_s}, h_2 = \frac{-L_m}{\delta L_s L_r}, \delta = 1 - \frac{L_m^2}{L_s L_r}. \end{aligned}$$

From model of induction motor, adaptive full order observer is given by (2)

$$\begin{cases} p\hat{\vec{\lambda}}_s = \hat{\boldsymbol{A}}_{\boldsymbol{11}}\hat{\vec{\lambda}}_s + \boldsymbol{A_{12}}\hat{\vec{\lambda}}_r + \boldsymbol{B}_v\vec{v}_s + \boldsymbol{G_1}\vec{e}_{is} \\ p\hat{\vec{\lambda}}_r = \boldsymbol{A_{21}}\hat{\vec{\lambda}}_s + \hat{\boldsymbol{A}}_{\boldsymbol{22}}\hat{\vec{\lambda}}_r + \boldsymbol{G}_2\vec{e}_{is} \\ \hat{\vec{i}}_s = \boldsymbol{H}_1\hat{\vec{\lambda}}_s + \boldsymbol{H}_2\hat{\vec{\lambda}}_r \end{cases} \tag{2}$$

where

$$\begin{aligned} \vec{e}_{is} &= \begin{bmatrix} i_{sd} - \hat{i}_{sd}, i_{sq} - \hat{i}_{sq} \end{bmatrix}^T \\ \hat{\boldsymbol{A}}_{\boldsymbol{11}} &= a_{11}\boldsymbol{I} + \hat{\omega}_e\boldsymbol{J}, \hat{\boldsymbol{A}}_{\boldsymbol{22}} = a_{22}\boldsymbol{I} + (\hat{\omega}_e - \hat{\omega}_r)\boldsymbol{J}. \end{aligned}$$

As indicated in [1], based on the error equation of stator and rotor flux in stator frame, the speed estimation algorithm can be

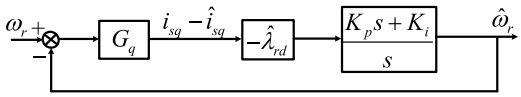

Fig. 2. Block diagram of traditional speed estimation algorithm.

TABLE II
PARAMETERS OF MOTOR AND OBSERVER

Symbol	PARAMETERS	Values
P_e	Rated Power	7.5 kW
V_e	Rated Voltage	380 V
I_e	Rated Current	15.6 A
f_e	Rated Frequency	50 Hz
n_e	Rated Speed	1470 r/min
P_n	Pole Pair	2
R_s	Stator Resistance	0.567 Ω
R_r	Rotor Resistance	0.441 Ω
L_m	Magnetizing Inductance	110.1 mH
L_s	Stator Self-Inductance	114.1 mH
L_r	Rotor Self-Inductance	114.1 mH

obtained through the Lyapunov's theorem

$$\hat{\omega}_r = \left(k_p + \frac{k_i}{s}\right)[(e_{\mathrm{is}\alpha}\hat{\lambda}_{r\beta} - e_{\mathrm{is}\beta}\hat{\lambda}_{r\alpha}) - (e_{\lambda r\alpha}\hat{\lambda}_{r\beta} - e_{\lambda r\beta}\hat{\lambda}_{r\alpha})]. \tag{3}$$

In classical speed estimation, it is also assumed that

$$\vec{\lambda}_r = \hat{\vec{\lambda}}_r. \tag{4}$$

And estimated speed is

$$\hat{\omega}_r = \left(k_p + \frac{k_i}{s}\right)(e_{\mathrm{is}\alpha}\hat{\lambda}_{r\beta} - e_{\mathrm{is}\beta}\hat{\lambda}_{r\alpha}). \tag{5}$$

In rotary reference frame, speed estimation is

$$\hat{\omega}_r = \left(k_p + \frac{k_i}{s}\right)(\hat{i}_{sq} - i_{sq})\hat{\lambda}_{rd}. \tag{6}$$

The closed-loop block diagram of speed estimation is shown as Fig. 2.

The open-loop transfer function (OLTF) between actual and estimated rotor speed can be derived from Fig. 2 as

$$G_{\mathrm{op}}(s) = -\hat{\lambda}_{rd}\left(K_P + \frac{K_I}{s}\right)G_q(s) \tag{7}$$

where $G_q(s)$ is indicated as (13).

Based on classical speed estimation, the design method for observer feedback gains has been researched for many years and lots of designed feedback gains have been obtained. Each feedback gain has its own advantage and disadvantage. In general there are three typical design methods for feedback gains [20]–[22]. In this section three different feedback gains are given based on the three design methods. Table II is the parameters of induction motor for design process. The advantages and disadvantages of these three methods are discussed. Summing up all the advantages and disadvantages of classical design methods, a robust design method is proposed and the system robustness and stability are improved in Section III.

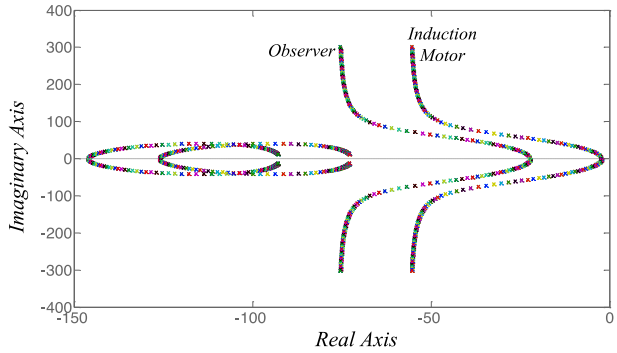

Fig. 3. Poles placement of observer and induction motor.

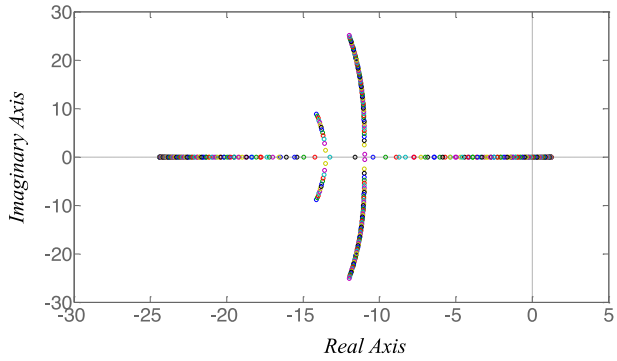

Fig. 4. Zeros of speed estimation transfer function.

A. Design Method Based on Pole Placement of Observer

Based on pole placement of observer, the feedback gains can be obtained in (8).

With (8) the pole placement of observer is shown in Fig. 3. Observer poles are moved to left from motor poles. Because motor poles are closer to imaginary axis, the convergence rate of observer is faster than motor. And the dynamic performance of observer can be well.

With (7) and (8), the zeros of OLTF with full load are shown in Fig. 4 ($-10\pi \le \omega_e \le 10\,\pi$). There are several zeros at right of plane (unstable zeros) when motor operates at low-speed regenerating mode. That means there are poles of closed loop transfer at right of plane, and speed estimation system is unstable.

$$\begin{cases} g_1 = kR_s\left(1 + \dfrac{a_{22}}{a_{11}}\right)(1 - \delta a_{22} f) \\ g_2 = -kR_s\left(1 + \dfrac{a_{22}}{a_{11}}\right) f\hat{\omega}_r \\ g_3 = -kR_s\dfrac{L_r}{L_m}\left(1 + \dfrac{a_{22}}{a_{11}}\right)(1 + \delta a_{22} f) \\ g_4 = -kR_s\dfrac{L_r}{L_m}\left(1 + \dfrac{a_{22}}{a_{11}}\right)\hat{\omega}_r \\ f = \dfrac{\delta a_{22} - (k+1)(a_{11} + a_{22})}{\omega_r^2 + (\delta a_{22})^2}. \end{cases} \tag{8}$$

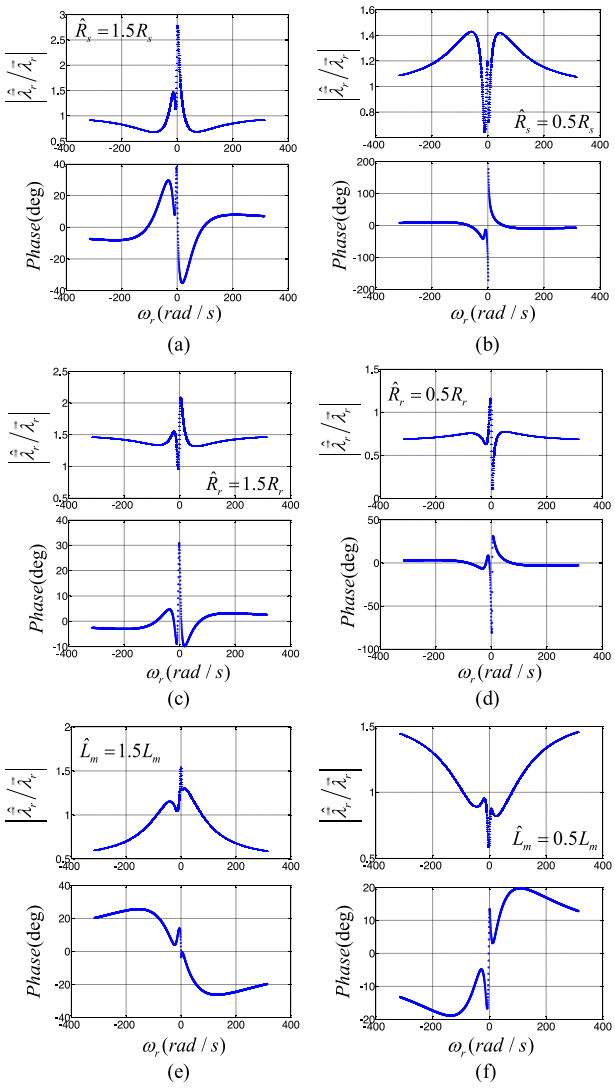

Fig. 5. Error between estimated and actual rotor flux using feedback gains of (8).

With (8) and dynamic model of observer and induction motor, complex vector $\hat{\vec{\lambda}}_r / \vec{\lambda}_r$ can be obtained. Fig. 5 shows the amplitude and phase error of estimated rotor flux with motor parameters deviation. When ω_r is negative, the motor operates in regenerating mode. It can be concluded from Fig. 5 that the influence of R_s is small in high speed range. With ω_r reducing the amplitude and phase error become large. R_r deviation mainly influences amplitude error. Phase error can be neglected. Only if rotor speed is near zero, phase error is enlarged sharply. The inaccurate L_m has strong influence on both amplitude and phase error, the error is too large to keep observer stable.

B. Design Method Based on Error of Estimated Rotor Flux

For minimum amplitude and phase error of estimation rotor flux, feedback gains can be obtained

$$g_1 \gg R_s,\ g_2 = 0,\ g_3 = L_m,\ g_4 = 0. \tag{9}$$

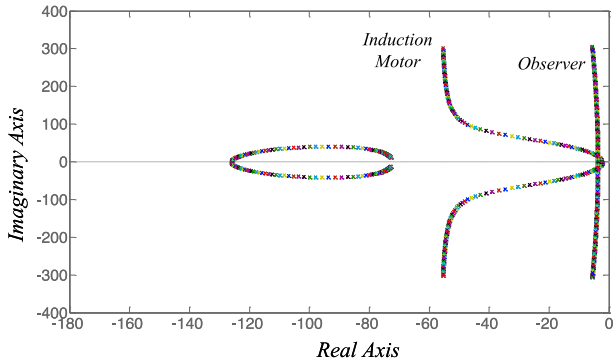

Fig. 6. Poles placement of observer and induction motor.

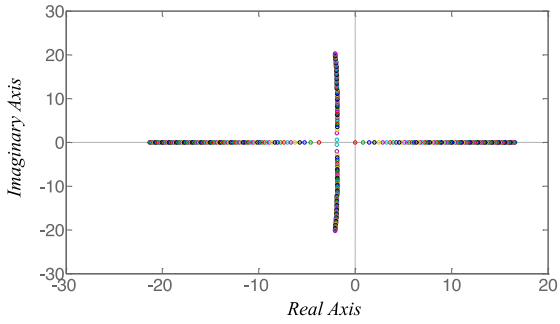

Fig. 7. Zeros of speed estimation transfer function.

With (9) the pole placement of observer is shown in Fig. 6. It can be seen that many poles with large imaginary part are closed to imaginary axis. That may result in instability in digital system [9]. To resolve this problem, the trapezoidal approximation for system discretization has to be used.

With (7) and (9) the zeros of OLTF with full load are shown in Fig. 7 $(-10\pi \le \omega_e \le 10\pi)$. There are still many unstable zeros.

With (9), the amplitude and phase error of estimated rotor flux are shown in Fig. 8. When ω_r is negative, the motor operates in regenerating mode. It can be seen from Fig. 8 that, inaccurate R_s used in observer do not cause error of rotor flux. Inaccurate L_m used in observer only causes small error when rotor speed is around zero. The influence of R_r is mainly on amplitude error, and only when rotor speed is around zero, phase error is caused.

C. Design Method Based on Stability of Estimated Speed

Based on stability of estimated speed, feedback gains can be obtained

$$\begin{cases} g_1 = \delta L_s \left[-\dfrac{R_s}{\delta L_s} - \dfrac{(1-\delta)\, R_r}{\delta L_r} + k\dfrac{R_r}{L_r} + \dfrac{R_r L_m^2}{L_r^2} \right] \\ g_2 = -k\delta L_s \hat{\omega}_r \\ g_3 = \dfrac{R_r L_m}{L_r} \\ g_4 = 0. \end{cases} \tag{10}$$

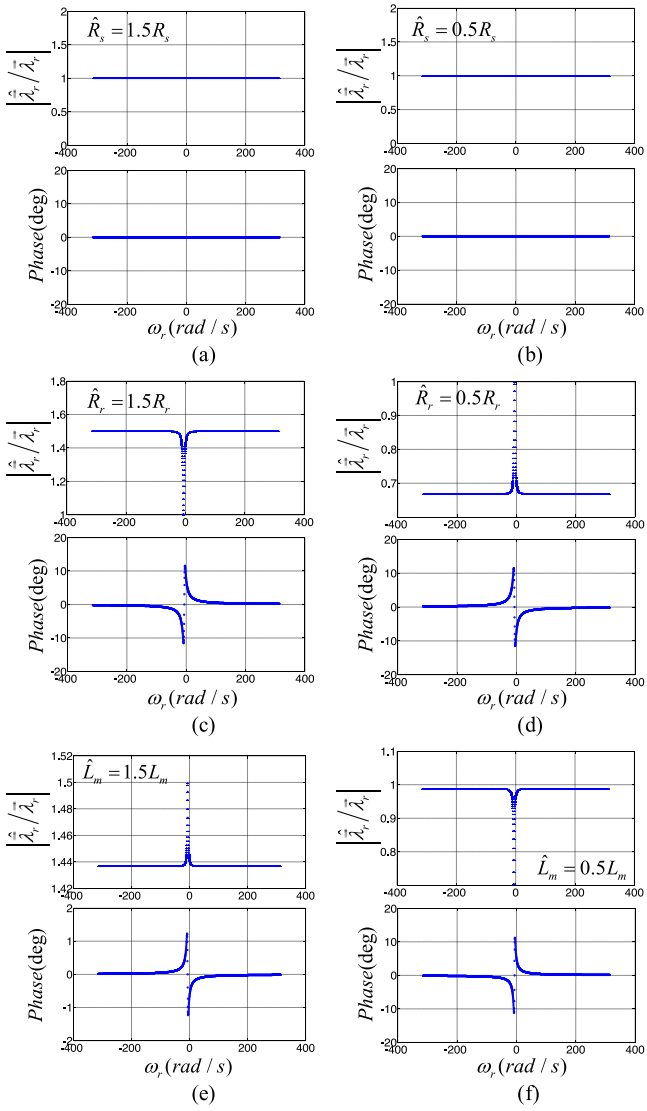

Fig. 8. Error between estimated and actual rotor flux using feedback gains of (9).

With (10) the pole placement of observer is shown in Fig. 9. Similar to Fig. 6 large imaginary part may result in instability in digital system.

With (7) and (10) the zeros of OLTF with full load are shown in Fig. 10 ($-10\pi \le \omega_e \le 10\pi$). It can be seen that there is no unstable zero at low-speed regenerating range. And speed estimation can be stable with full load at all speed range.

With (10), the amplitude and phase error of estimated rotor flux are shown in Fig. 11. When ω_r is negative, the motor operates in regenerating mode. It can be seen from Fig. 11 that the stator resistance error has no influence on the amplitude and phase of estimated rotor flux. For rotor field oriented control, the phase error has more influence on drive performance. However, the estimated rotor flux phase error caused by rotor resistance error is small that can be neglected in application. Compared with (9) the phase error caused by L_m is larger. It is noted that the feedback gains (10) can guarantee the stability of speed

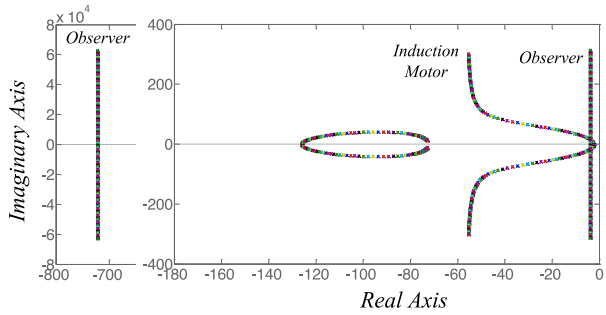

Fig. 9. Poles placement of observer and induction motor.

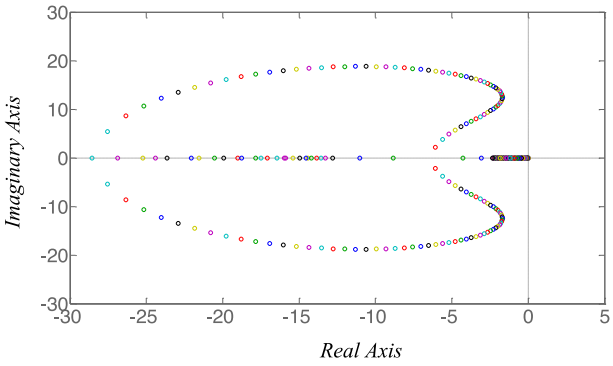

Fig. 10. Zeros of speed estimation transfer function.

estimation and minimum estimated flux error. However, the performance can be improved further if feedback gains or speed estimation algorithm is improved. Those are mainly discussed in Sections III and IV.

III. Classical Speed Estimation and Robust Feedback Gains

The stability is the most important performance for the estimation system. So the design for robust feedback gains is based on stability of speed estimation in this manuscript. For simplifying analysis, (2) and (3) are improved to be indicated in complex form.

$$\frac{d}{dt}\begin{bmatrix}\hat{\vec{\lambda}}_s\\ \hat{\vec{\lambda}}_r\end{bmatrix} = \boldsymbol{A}\begin{bmatrix}\hat{\vec{\lambda}}_s\\ \hat{\vec{\lambda}}_r\end{bmatrix} + \begin{bmatrix}\vec{v}_s\\ 0\end{bmatrix} + \boldsymbol{G}_c\Delta\vec{i}_s \tag{11}$$

$$\frac{d}{dt}\begin{bmatrix}\vec{\lambda}_s - \hat{\vec{\lambda}}_s\\ \vec{\lambda}_r - \hat{\vec{\lambda}}_r\end{bmatrix} = \boldsymbol{A}\begin{bmatrix}\vec{\lambda}_s - \hat{\vec{\lambda}}_s\\ \vec{\lambda}_r - \hat{\vec{\lambda}}_r\end{bmatrix} - \boldsymbol{G}_c\Delta\vec{i}_s + \begin{bmatrix}0\\ j\hat{\vec{\lambda}}_r\end{bmatrix}\Delta\omega_r \tag{12}$$

where

$$\boldsymbol{A} = \begin{bmatrix}a_{11} - j\omega_e & a_{13}\\ a_{31} & a_{33} - j(\omega_e - \hat{\omega}_r)\end{bmatrix}, \boldsymbol{G}_c = \begin{bmatrix}g_1 - jg_2\\ g_3 - jg_4\end{bmatrix}$$

$$\Delta\vec{i}_s = \left(i_{sd} - \hat{i}_{sd}\right) + j\left(i_{sq} - \hat{i}_{sq}\right), \Delta\omega_r = \omega_r - \hat{\omega}_r.$$

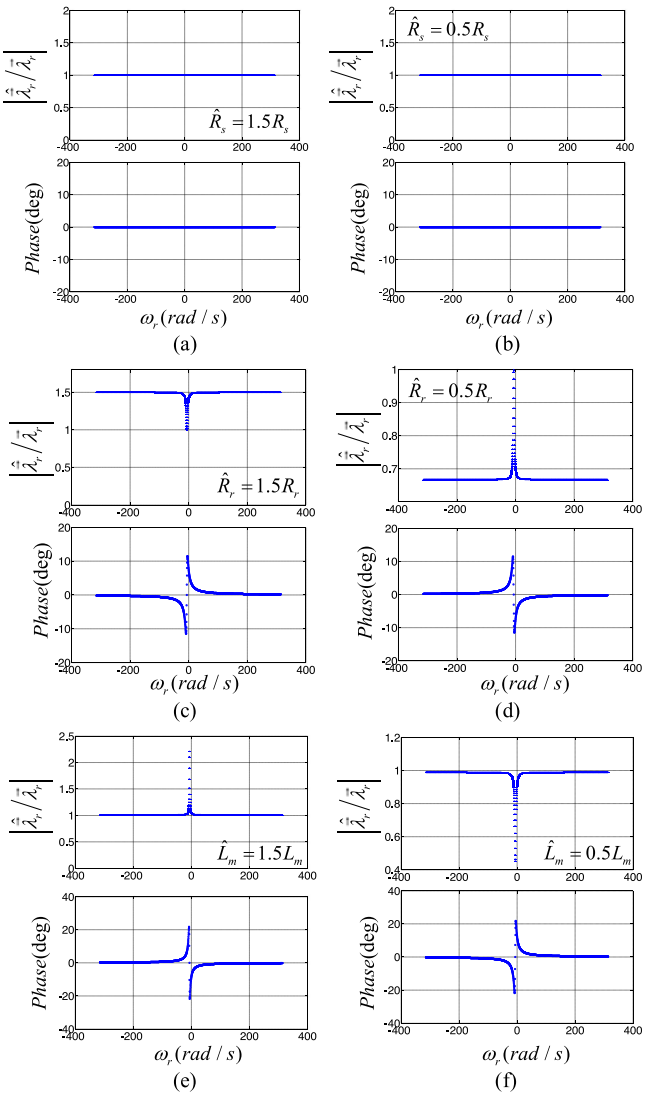

Fig. 11. Error between estimated and actual rotor flux using feedback gains of (10).

Derived from (12)

$$G_q(s) = \frac{i_{sq} - \hat{i}_{sq}}{\Delta\omega_r} = \frac{s^3 + q_2 s^2 + q_1 s + q_0}{B} \tag{13}$$

$$G_d(s) = \frac{i_{sd} - \hat{i}_{sd}}{\Delta\omega_r} = \frac{d_2 s^2 + d_1 s + d_0}{B} \tag{14}$$

where

$$\begin{aligned}
B &= s^4 + b_3 s^3 + b_2 s^2 + b_1 s + b_0 \\
q_2 &= \frac{L_r(R_s + g_1) + R_r L_s - g_3 L_m}{\delta L_s L_r} = x \\
q_1 &= \omega_e^2 + \frac{g_1 R_r + R_s R_r}{\delta L_s L_r} - \frac{g_2 \omega_r}{\delta L_s} = \omega_e^2 + y \\
q_0 &= \frac{L_r(R_s + g_1) + R_r L_s - g_3 L_m}{\delta L_s L_r}\omega_e^2 \\
&\quad - \left(\frac{g_2 R_r}{\delta L_s L_r} + \frac{R_s + g_1}{\delta L_s}\omega_r\right)\omega_e \\
&= x\omega_e^2 + z\omega_e \\
d_2 &= \frac{-g_4 L_m^2}{\delta^2 L_s^2 L_r^2} + \frac{g_2 L_m}{\delta^2 L_s^2 L_r} - \frac{L_m(\omega_e - \omega_r)}{\delta L_s L_r} \\
d_1 &= \frac{R_s L_m + g_1 L_m}{\delta^2 L_s^2 L_r}\omega_r + \frac{g_2 R_r L_m}{\delta^2 L_s^2 L_r^2} \\
d_0 &= \frac{-\omega_e^2 L_m(\omega_e - \omega_r)}{\delta L_s L_r} - \frac{\omega_e^2 L_m^2 g_4 - \omega_e L_m R_r(R_s + g_1)}{\delta^2 L_s^2 L_r^2} \\
&\quad + \frac{\omega_e L_m g_2(\omega_e - \omega_r)}{\delta^2 L_s^2 L_r}.
\end{aligned}$$

The closed-loop block diagram of speed estimation is shown as Fig. 2. To guarantee the stability of speed estimation, all the zeros of OLTF have to be located in the left plane. With (7) and (13) and applying Routh–Hurwitz criterion, the Routh Table is as

s^3	1	q_1
s^2	q_2	q_0
s^1	$q_1 - \frac{q_0}{q_2}$	0
s^0	q_0	0

With Routh Table, the necessary and sufficient conditions for the stability of speed estimation can be obtained

$$\begin{cases} x > 0 \\ xy - z\omega_e > 0 \\ x\omega_e^2 + z\omega_e > 0. \end{cases} \tag{15}$$

It is difficult to obtain the value of feedback $\boldsymbol{G}_c$, because the x, y and z in (15) are complicated. Neglecting the second condition in (15) for simple analysis, the feedback gains (10) can be obtained. In this paper, all the conditions are considered. To satisfy (15), condition (16) is obtained

$$\begin{cases} x > 0 \\ y > 0 \\ z = 0. \end{cases} \tag{16}$$

1) $z = 0$. Based on this equation, the relationship between g_1 and g_2 can be obtained

$$g_2 = \frac{-L_r(R_s + g_1)\omega_r}{R_r}. \tag{17}$$

2) $y > 0$. Based on this condition, a range of g_1 for speed estimation stability can be obtained

$$g_1 > -R_s. \tag{18}$$

3) $x > 0$. Based on this condition, relationship between g_1 and g_3 can be obtained

$$g_1 > \frac{L_m}{L_r} g_3. \tag{19}$$

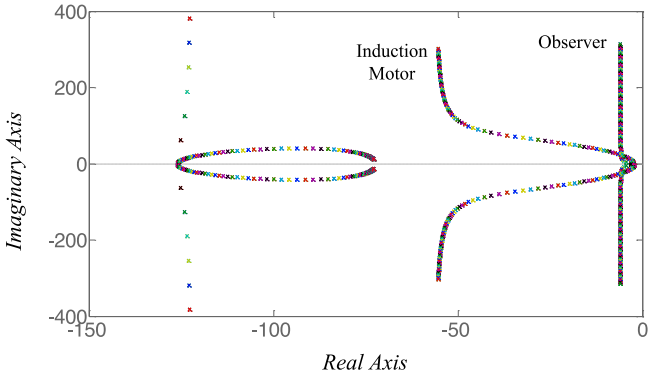

Fig. 12. Poles placement of observer and induction motor.

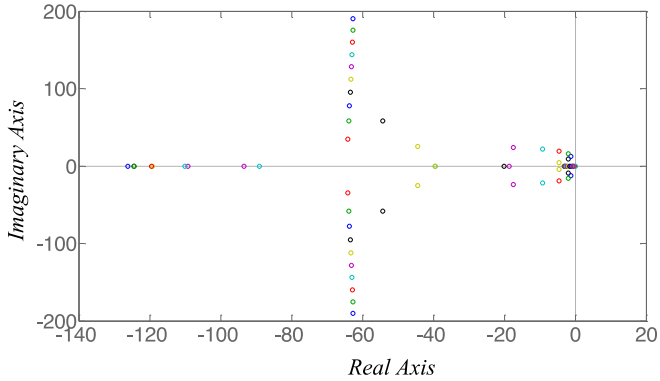

Fig. 13. Zeros of speed estimation transfer function.

Finally the necessary and sufficient conditions for the stability of speed estimation can be obtained

$$\begin{cases} g_2 = \dfrac{-L_r\left(R_s + g_1\right)\omega_r}{R_r} \\ g_1 > \dfrac{L_m}{L_r} g_3 > -R_s. \end{cases} \tag{20}$$

If feedback gains satisfy (20), the stability of speed estimation can be guaranteed at all speed range. It can be seen from (20), g_4 has no influence on stability of speed estimation. In this paper, the feedback gains are given for simplicity as

$$\begin{cases} g_1 = g_3 = 0.05 \\ g_2 = \dfrac{-L_r\left(R_s + g_1\right)\omega_r}{R_r} \\ g_4 = 0. \end{cases} \tag{21}$$

With (21) the pole placement of observer and induction motor are shown in Fig. 12. It can be seen that many poles with large imaginary part are closed to imaginary axis. That may result in instability in digital system [9]. To resolve this problem, the trapezoidal approximation for system discretization has to be used.

With (7) and (21) the zeros of OLTF with full load are shown in Fig. 13 ($-10\pi \leq \omega_e \leq 10\,\pi$). It is noted that there is no unstable zero at low speed regenerating range. And speed estimation can be stable with full load at all speed range.

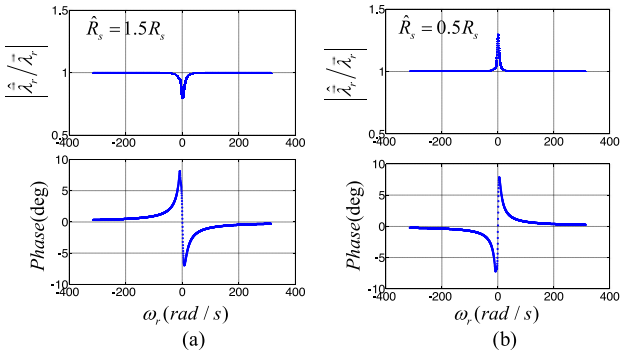

Fig. 14. Error between estimated and actual rotor flux using feedback gains of (21).

With (21), the amplitude and phase error of estimated rotor flux are shown in Fig. 14. When ω_r is negative, the motor operates in regenerating mode. Compared with feedback gains (10), estimated rotor flux is sensitive to R_s but the estimated flux error is small that can be ignored. The sensitivity of estimated rotor flux to R_r and L_m is as same as (10).

From above analysis of feedback gains (21), the performance is similar to the performance of feedback gains (10). However, with (21) the estimated speed error can be reduced. Figs. 15 and 16 indicate the relationship among estimated speed error, ω_e and the load with motor parameters deviation. Because in most industry applications, the largest parameter error that can be reached is $\pm 50\%$, the parameters error is $\pm 50\%$ in the analysis. When the load torque is negative, the motor is running in regenerating mode.

1) Comparison when $R_s - \hat{R}_s = +50\%$. Except low speed range ($0 < \omega_e < 10\pi$), the stator resistance deviation has no influence on speed estimation. But at low speed range especially when the motor runs in regenerating mode, the estimated speed error enlarges sharply when load enlarges. With (10), the maximum estimated speed error is –18 rad/s. But the maximum estimated speed error is reduced to -10 rad/s with (21).
2) Comparison when $R_s - \hat{R}_s = -50\%$. Similar to the first analysis the maximum estimated speed error is reduced with (21).
3) Comparison when $R_r - \hat{R}_r = +50\%$. At middle and high speed range ($\omega_e > 10\pi$), the estimated speed error is only related with load. The larger the load is, the larger the estimated speed error is. However at low speed range ($0 < \omega_e < 10\pi$), the estimated speed error turns large sharply. With (10), the maximum estimated speed error is -25 rad/s. But the maximum estimated speed error is reduced to -11 rad/s with (21). The proposed feedback gain has strong robustness to rotor resistance deviation.
4) Comparison when $R_r - \hat{R}_r = -50\%$. There is no obviously difference of performance between (10) and (21). The estimated speed error is related with load. At low speed range the maximum estimated speed error is 7 rad/s with (10) but is 6 rad/s with (21).

With proposed feedback gains, the estimated speed sensitivity to rotor and stator resistance can be reduced by half. But

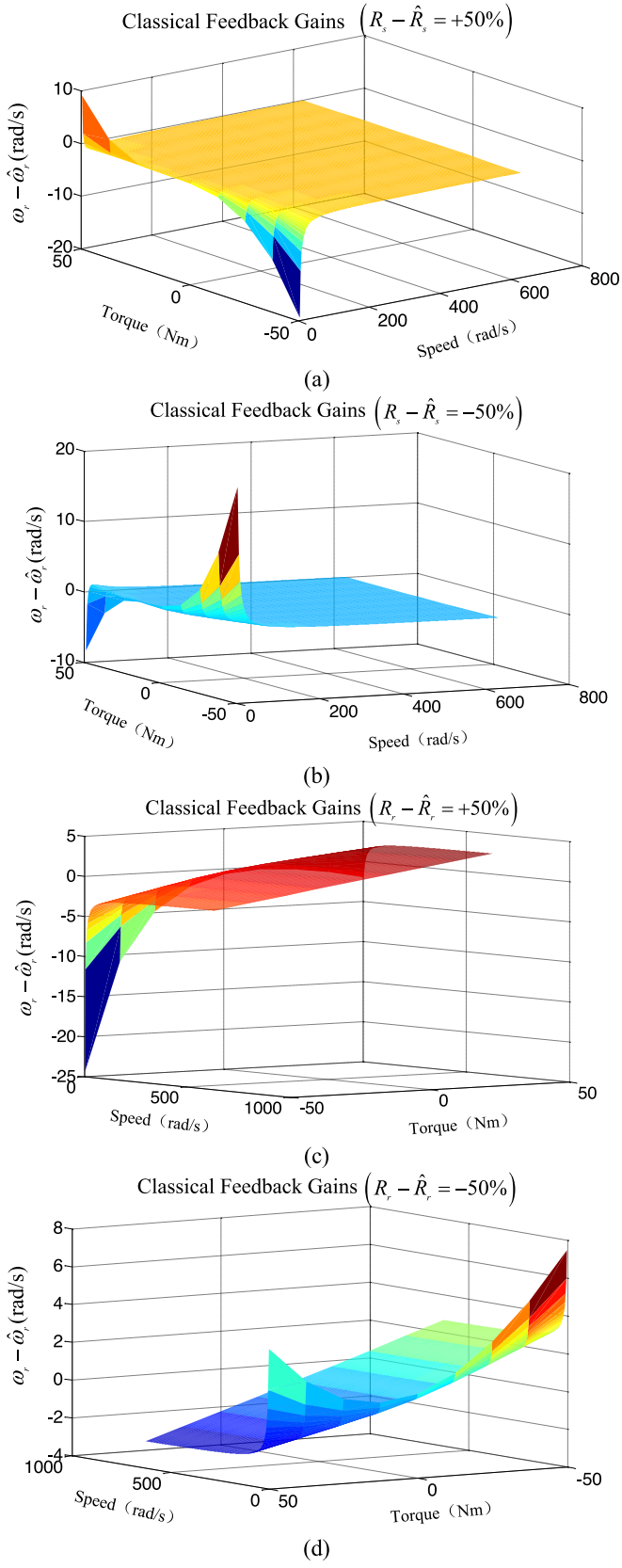

Fig. 15. Estimated speed error with motor parameter deviation, classical speed estimation algorithm and classical feedback gains.

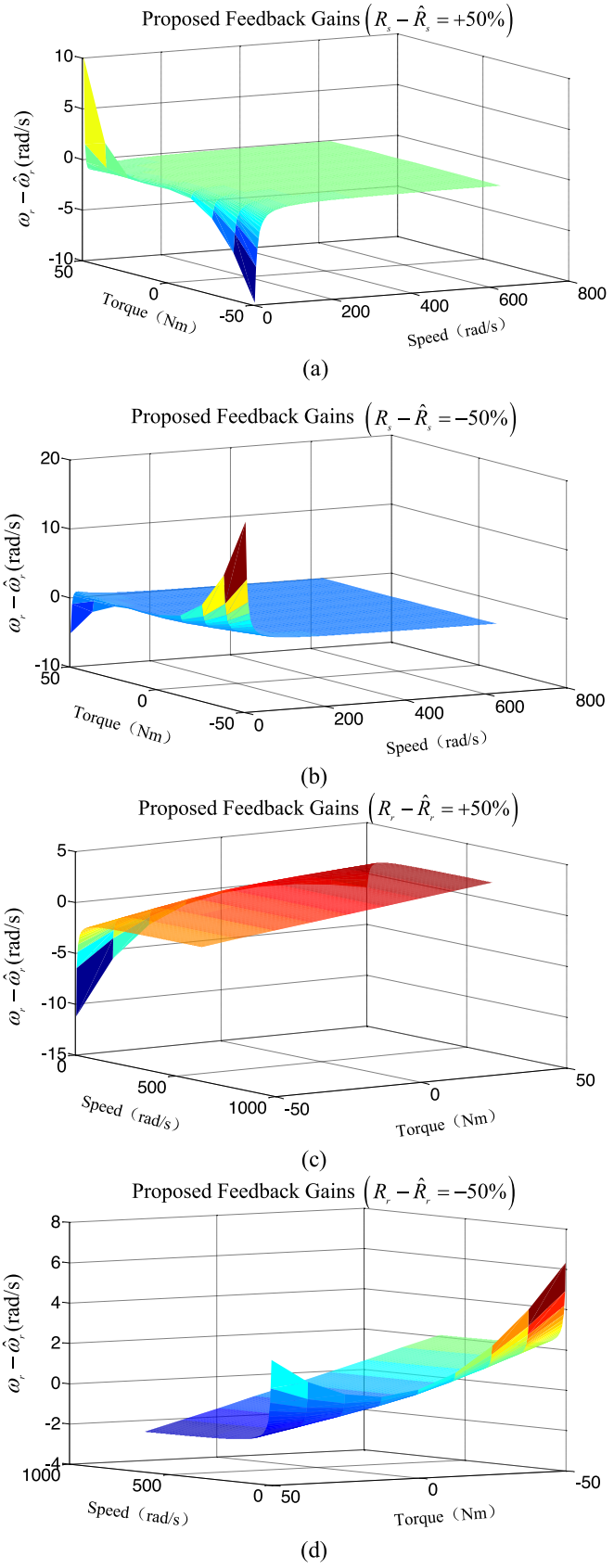

Fig. 16. Estimated speed error with motor parameter deviation, classical speed estimation algorithm and robust feedback gains.

with a robust speed estimation algorithm, which is proposed in next section, the estimated speed sensitivity to rotor and stator resistance can be reduced further more.

IV. Robust Speed Estimation and Robust Feedback Gains Design Method

In classical speed estimation algorithm, the estimated rotor flux error is ignored because the actual rotor flux can not be measured in industry application. However, the estimated rotor flux error has strong influence on speed estimation stability and robustness to motor parameter deviation. It is necessary to introduce the estimated rotor flux error to speed estimation algorithm.

A. Robust Speed Estimation With Classical Feedback Gains

Because real rotor flux can not be measured in practical application the form of estimated rotor flux error in (3) needs to be improved. In (3)

$$e_{\lambda r\alpha} = \lambda_{r\alpha} - \hat{\lambda}_{r\alpha}, e_{\lambda r\beta} = \lambda_{r\beta} - \hat{\lambda}_{r\beta}.$$

Rotor flux error in stationary reference frame in (3) is

$$E_{\mathrm{flx\_}s} = e_{\lambda r\alpha}\hat{\lambda}_{r\beta} - e_{\lambda r\beta}\hat{\lambda}_{r\alpha} = \lambda_{r\alpha}\hat{\lambda}_{r\beta} - \lambda_{r\beta}\hat{\lambda}_{r\alpha}. \quad (22)$$

Extracting the same factor $\sqrt{\lambda_{r\alpha}^2+\lambda_{r\beta}^2}\cdot\sqrt{\hat{\lambda}_{r\alpha}^2+\hat{\lambda}_{r\beta}^2}$, (22) can be derived as

$$\begin{aligned} E_{\mathrm{flx\_}s} =& \sqrt{\lambda_{r\alpha}^2+\lambda_{r\beta}^2}\cdot\sqrt{\hat{\lambda}_{r\alpha}^2+\hat{\lambda}_{r\beta}^2} \\ &\times\left(\frac{\lambda_{r\alpha}\hat{\lambda}_{r\beta}-\lambda_{r\beta}\hat{\lambda}_{r\alpha}}{\sqrt{\lambda_{r\alpha}^2+\lambda_{r\beta}^2}\cdot\sqrt{\hat{\lambda}_{r\alpha}^2+\hat{\lambda}_{r\beta}^2}}\right) \\ =& |\vec{\lambda}_r||\hat{\vec{\lambda}}_r|\left(\frac{\lambda_{r\alpha}}{|\vec{\lambda}_r|}\cdot\frac{\hat{\lambda}_{r\beta}}{|\hat{\vec{\lambda}}_r|}-\frac{\lambda_{r\beta}}{|\vec{\lambda}_r|}\cdot\frac{\hat{\lambda}_{r\alpha}}{|\hat{\vec{\lambda}}_r|}\right) \\ =& \left(|\hat{\vec{\lambda}}_r|^2+\Delta\lambda|\hat{\vec{\lambda}}_r|\right)\left(\sin\hat{\theta}\cos\theta-\cos\hat{\theta}\sin\theta\right) \end{aligned} \quad (23)$$

Defining θ as actual rotor flux angle, error between actual and estimated rotor flux angle is represented by $\Delta\theta$, error between actual and estimated rotor flux amplitude is represented by $\Delta\lambda$, and (23) can be derived as

$$E_{\mathrm{flx\_}s} = -\sin\Delta\theta\left(|\hat{\vec{\lambda}}_r|^2+\Delta\lambda|\hat{\vec{\lambda}}_r|\right). \quad (24)$$

According to Fig. 17, rotation speed of rotor flux vector is as same as rotation speed of stator current vector, and is also equal to rotation speed of rotor reference frame. Consequently, $\sin\Delta\theta$ is given

$$\sin\Delta\theta = \frac{|i_{sq}\hat{i}_{sd}-i_{sd}\hat{i}_{sq}|}{|\vec{i}_s|\cdot|\hat{\vec{i}}_s|}. \quad (25)$$

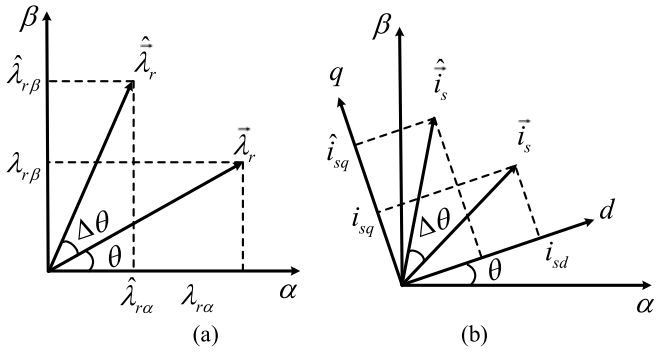

Fig. 17. Vector graphs of rotor flux and stator current.

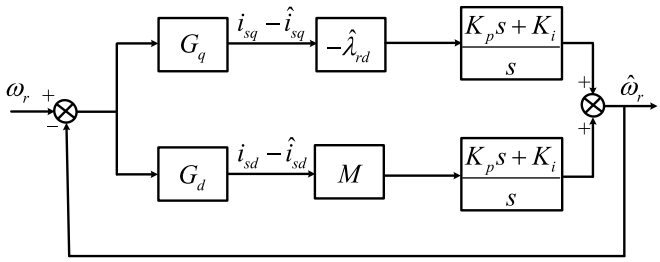

Fig. 18. Block diagram of proposed speed estimation algorithm.

In stationary frame, $\sin\Delta\theta$ is

$$\sin\Delta\theta = \frac{i_{s\alpha}\hat{i}_{s\beta}-i_{s\beta}\hat{i}_{s\alpha}}{\sqrt{2|\vec{i}_s|\cdot|\hat{\vec{i}}_s|\left(|\vec{i}_s|\cdot|\hat{\vec{i}}_s|+i_{s\alpha}\hat{i}_{s\alpha}+i_{s\beta}\hat{i}_{s\beta}\right)}}. \quad (26)$$

Ignoring $\Delta\lambda$ and introducing coefficient *M* in (24), the robust speed estimation algorithm is given as

$$\begin{aligned} \hat{\omega}_r =& \left(k_p+\frac{k_i}{s}\right)[(e_{\mathrm{is}\alpha}\hat{\lambda}_{r\beta}-e_{\mathrm{is}\beta}\hat{\lambda}_{r\alpha}) \\ &-M(i_{s\alpha}\hat{i}_{s\beta}-i_{s\beta}\hat{i}_{s\alpha})]. \end{aligned} \quad (27)$$

To simplify the analysis, the speed estimation algorithm in rotor-flux reference frame can be derived as

$$\hat{\omega}_r = -\left(k_p+\frac{k_i}{s}\right)[\hat{\lambda}_{rd}(i_{sq}-\hat{i}_{sq})-M(i_{sd}-\hat{i}_{sd})]. \quad (28)$$

Fig. 18 depicted the block diagram of proposed speed estimation algorithm. Compared with classical speed estimation algorithm, the transfer function $G_d(s)$ and coefficient *M* are added.

As indicated in Fig. 18, the OLTF $G_{\mathrm{op\_new}}$ of estimated speed is

$$G_{\mathrm{op\_new}}(s) = \left(K_P+\frac{K_I}{s}\right)\left[-\hat{\lambda}_{rd}G_q(s)+MG_d(s)\right]. \quad (29)$$

It is well known that when feedback gains are zero, there are unstable region of speed estimation when motor runs at low

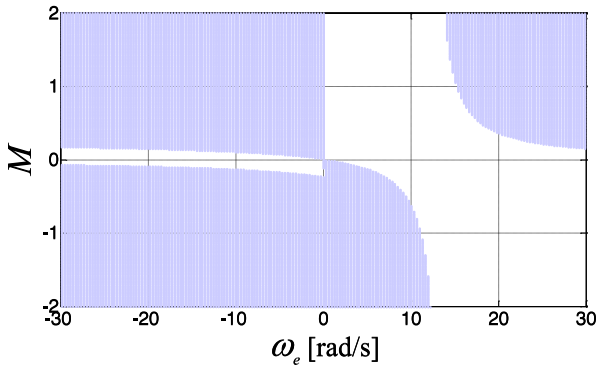

Fig. 19. Stable value of *M* for speed estimation stability at all speed range.

speed regenerating range. However, if *M* is designed properly, the speed estimation can be stable at all speed range. The detailed analysis can be found in [27].

Considering the stability of speed estimation, the real part of zeros and poles of OLTF $G_{\text{op\_new}}$ have to be negative. In order to find out the value of *M* that can guarantee the stability of speed estimation, Fig. 19 is obtained.

In Fig. 19, when ω_e is negative, the motor is running in regenerating mode. The white area represents the stable value of *M* that can guarantee the stability of speed estimation. And the shade means the unstable value of *M*. It can be seen that to guarantee the stability of speed estimation at all speed range, the stable range of *M* is from 0 to 0.1. In this paper and based on (24), (26) and Table II, the *M* can be calculated as 0.08.

Guaranteeing the stability of speed estimation is one function of *M*. The other function is improving the system robustness to motor parameter deviation. Based on classical feedback gains (10) the estimated speed error with parameter deviation is indicated in Fig. 15. To verify the feasibility how system robustness to parameter deviation is improved with proposed speed estimation algorithm, the feedback gains (10) are used again. But the speed estimation algorithm (27) is used instead of (5). The estimated speed error with parameter deviation is indicated in Fig. 20, where *M* is 0.08.

1) When $R_s - \hat{R}_s = \pm 50\%$. Compared with Fig. 15, it can be seen that with same feedback gains (10), the estimated speed error, especially at low speed range, is reduced by half when proposed speed estimation is used.
2) When $R_r - \hat{R}_r = \pm 50\%$. Compared with Fig. 15, when (10) and proposed speed estimation (27) are used, the estimated speed error at low speed range is reduced much more.

B. Robust Speed Estimation With Corresponding Robust Feedback Gains

To design the feedback gains, the stability of speed estimation is considered first. In the same way to guarantee the stability of speed estimation, all the zeros of (29) have to be in the left plane.

For simplicity, $M = \hat{\lambda}_{rd}$ and (29) is improved as

$$G_{\text{op\_new}}(s) = \frac{(K_P s + K_I)}{Bs}\left[s^3 + p_2 s^2 + p_1 s + p_0\right] \quad (30)$$

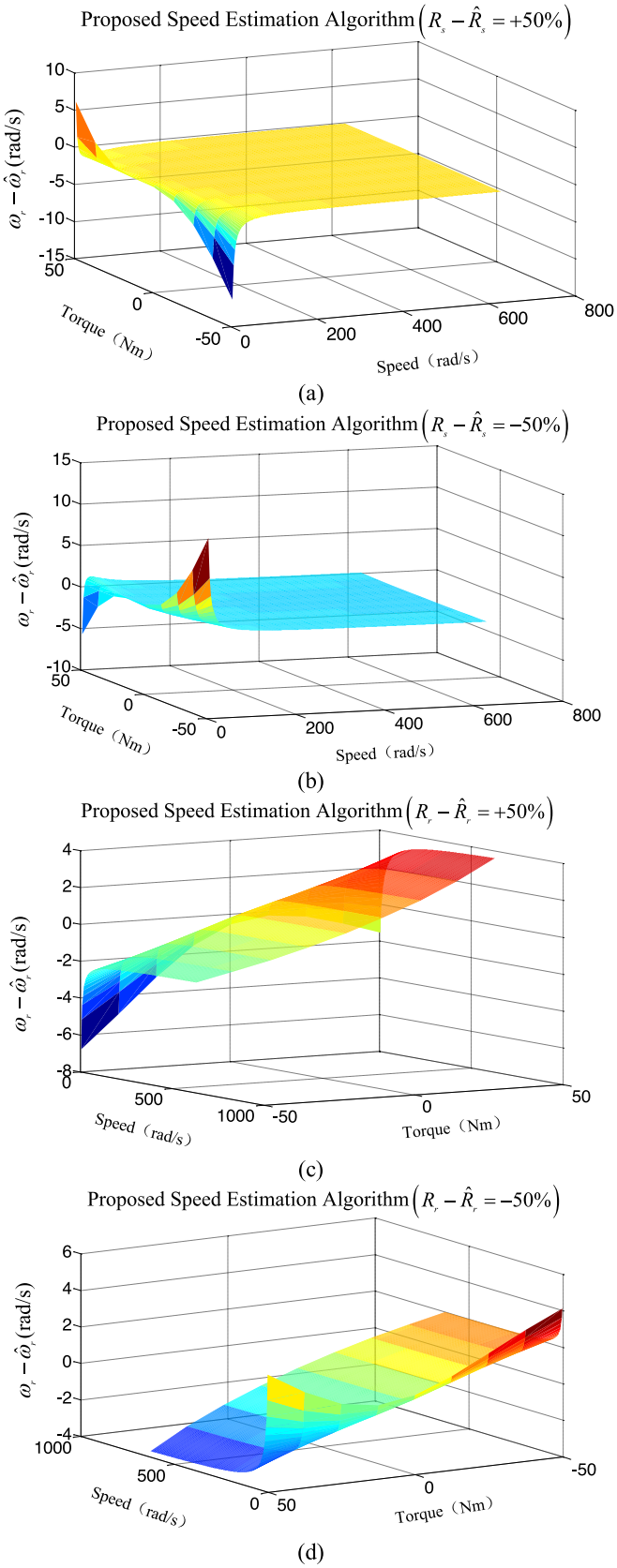

Fig. 20. Estimated speed error with motor parameter deviation, robust speed estimation algorithm and classical feedback gains.

where

$$\begin{aligned} p_2 &= q_2 - d_2 = A_3\omega_e + A_2 \\ p_1 &= q_1 - d_1 = \omega_e^2 + A_1 \\ p_0 &= q_0 - d_0 = A_3\omega_e^3 + A_2\omega_e^2 + A_0\omega_e. \end{aligned}$$

Applying Routh–Hurwitz criterion, the Routh Table can be obtained

s^3	1	p_1
s^2	p_2	p_0
s^1	$p_1 - \frac{p_0}{p_2}$	0
s^0	p_0	0

With Routh Table the necessary and sufficient conditions for the stability of speed estimation can be obtained

$$\begin{cases} A_3\omega_e + A_2 > 0 \\ A_1 - \dfrac{A_0\omega_e}{A_3\omega_e + A_2} > 0 \\ \omega_e^2\left(A_3\omega_e + A_2\right) + A_0\omega_e > 0. \end{cases} \tag{31}$$

To satisfy (31), condition (32) is obtained

$$\begin{cases} A_0 = 0 \\ A_1 > 0 \\ A_3\omega_e + A_2 > 0. \end{cases} \tag{32}$$

1) $A_0 = 0$. Based on this equation, the relationship between g_1 and g_2 can be obtained

$$g_2 = \frac{\delta L_s L_r^2\omega_r + L_m R_r}{L_r L_m\omega_r - \delta L_s L_r R_r}\left(R_s + g_1\right). \tag{33}$$

2) $A_1 > 0$. Based on this condition, a range of g_2 for speed estimation stability can be obtained

$$\frac{g_2}{L_r\omega_r + \frac{L_m R_r}{\delta L_s L_r}} < 0. \tag{34}$$

It can be found based on motor parameters in Table II, when $-100\pi < \omega_r < 100\,\pi$, the denominator of (34) is always positive. So (34) can be satisfied as long as g_2 is negative. However, this feedback gains only can be applied in fundamental speed range (within $\pm$50 Hz).

3) $A_3\omega_e + A_2 > 0$. Based on this condition the relationship between slip frequency and feedback gains can be obtained

$$\begin{aligned} \omega_e - \omega_r > &\left(\frac{1}{\delta L_s} - \frac{\frac{L_r}{\delta L_s}\omega_r - \frac{L_r R_r}{L_m}}{L_r\omega_r + \frac{L_m R_r}{\delta L_s L_r}}\right) g_2 \\ &- \frac{L_m}{\delta L_s L_r} g_4 - \frac{R_r L_s - L_m g_3}{L_m}. \end{aligned} \tag{35}$$

TABLE III
ESTIMATED SPEED ERROR OF DIFFERENT METHODS FOR ADAPTIVE FULL ORDER OBSERVER

	R_s		R_r	
	+50%	−50%	+50%	−50%
CC	−18 rad/s	18 rad/s	−25 rad/s	7 rad/s
CR	−10 rad/s	10 rad/s	−11 rad/s	6 rad/s
RC	−10 rad/s	10 rad/s	−7 rad/s	4 rad/s
RR	1.2 rad/s	−1.2 rad/s	−0.16 rad/s	0.16 rad/s

Similarly when $-100\pi < \omega_r < 100\pi$ (within $\pm$ 50 Hz)

$$\frac{1}{\delta L_s} - \frac{\frac{L_r}{\delta L_s}\omega_r - \frac{L_r R_r}{L_m}}{L_r\omega_r + \frac{L_m R_r}{\delta L_s L_r}} > 0. \tag{36}$$

Because g_2 is negative, condition (35) can be satisfied as long as $g_3 < 0, g_4 > 0$ and all right terms of (35) are less than minimum slip frequency which is negative because the motor runs in regenerating mode.

Finally the necessary and sufficient conditions for the stability of speed estimation can be obtained

$$\begin{cases} g_1 = -L_m L_r\omega_r + \delta L_s L_r R_r - R_s \\ g_2 = -\delta L_s L_r^2\omega_r - L_m R_r \\ g_3 = k \\ g_4 = -k \end{cases} \quad (k < 0) \tag{37}$$

where k is the minimum slip frequency which is negative. In this paper, $k = -15$.

With the proposed speed estimation algorithm and corresponding feedback gains, the estimated speed error with parameter deviation is indicated in Fig. 21. When the load torque is −50 Nm and the reference ω_e is 4 rad/s in Figs. 15, 16, 20 and 21, the estimated speed error of different methods are indicated in Table III. It can be seen that the estimated speed error is almost zero and can be ignored when proposed speed estimation and corresponding feedback gains are used together.

CC: Classical speed estimation (5) and classical feedback gains (10).

CR: Classical speed estimation (5) and robust feedback gains (21).

RC: Robust speed estimation (27) and classical feedback gains (10).

RR: Robust speed estimation (27) and corresponding robust feedback gains (37).

With (37), the pole placement of observer is shown inFig. 22. Compared with feedback gains (10), there is no pole closed to imaginary axis with large imaginary part. The problem of instability in digital system is resolved.

With (27) and (37) the zeros of OLTF with full load are shown in Fig. 23 ($-10\pi \le \omega_e > 10\pi$). $M = 1$. It is noted that there is no unstable zero at low speed regenerating range. And speed estimation can be stable with full load at all speed range.

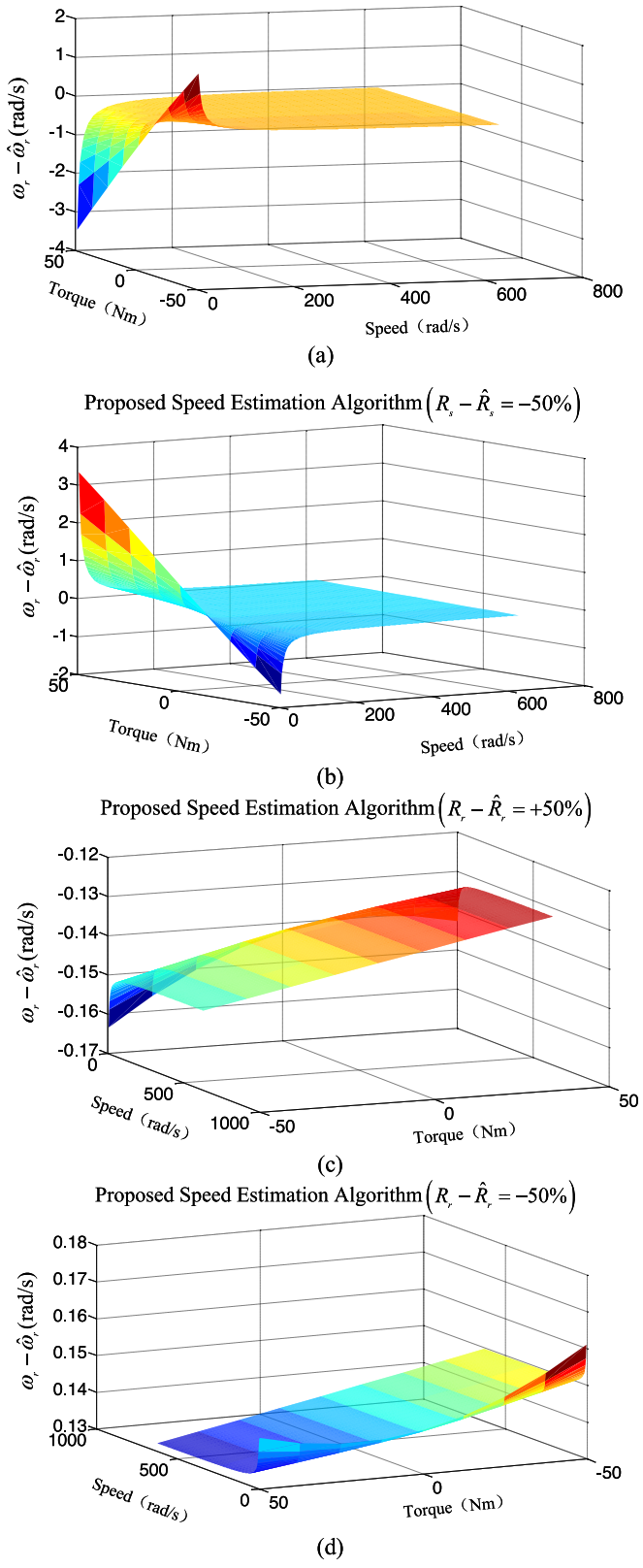

Fig. 21. Estimated speed error with motor parameter deviation, robust speed estimation algorithm and corresponding robust feedback gains.

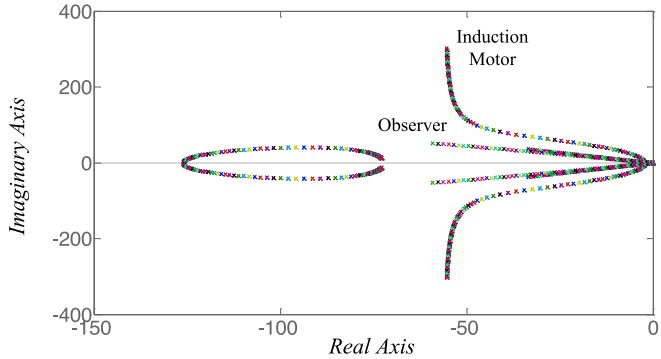

Fig. 22. Poles placement of observer and induction motor.

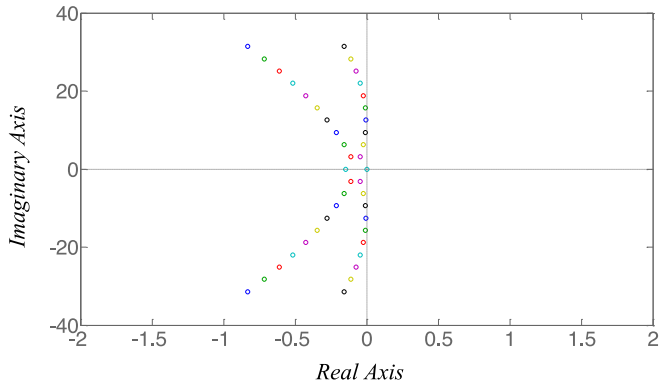

Fig. 23. Zeros of speed estimation transfer function.

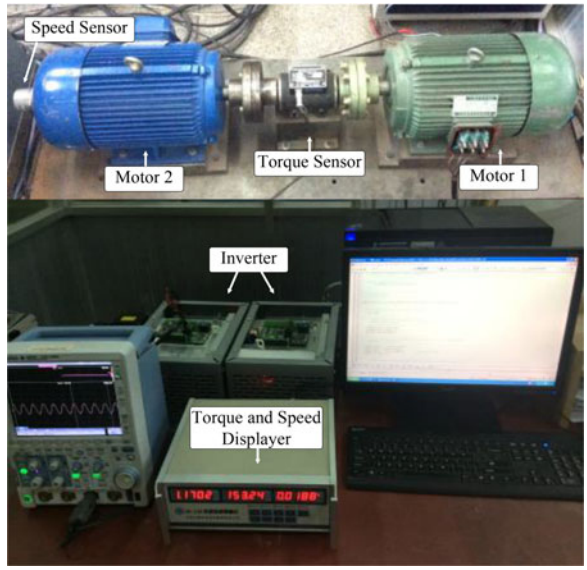

Fig. 24. Experiment platform.

V. Experimental Results

The proposed methods are verified using an experiment platform with STM32F103 ARM. The experimental platform, which is indicated in Fig. 24, adopts two 7.5-kW induction motors. Motor 1 is the tested motor and is controlled by sensorless

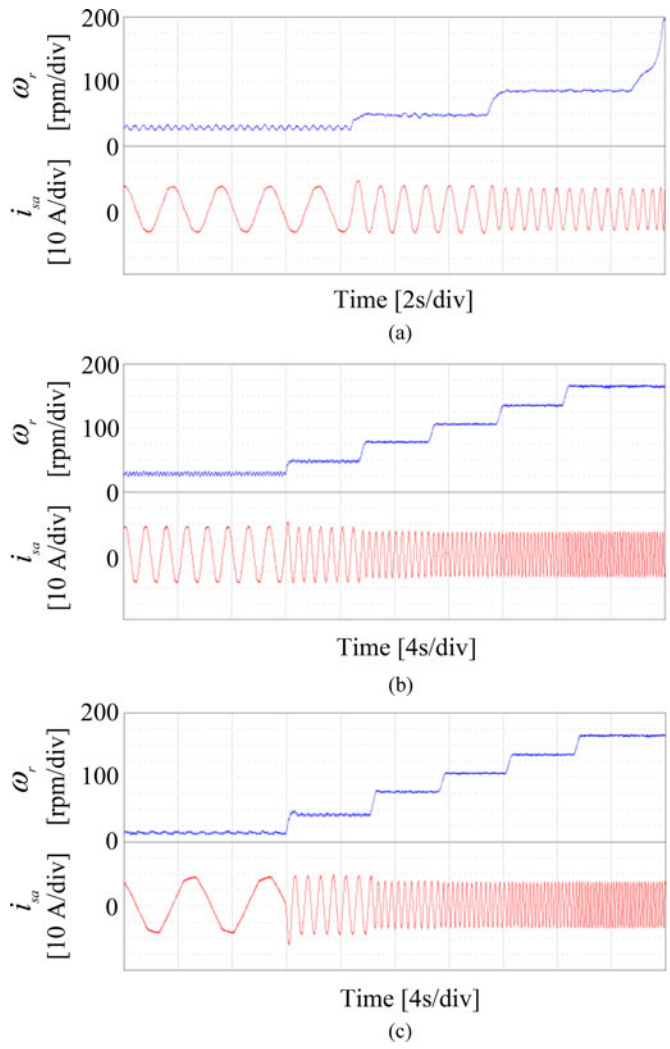

Fig. 25. Stability of speed estimation at low-speed regenerating range, 100% rated load. (a) Zero feedback gains and classical speed estimation. (b) Robust feedback gains and classical speed estimation. (c) Robust feedback gains and robust speed estimation.

vector control. Motor 2 is the load motor offering torque for Motor 1 and is controlled with speed encoder. The parameters of Motor 1 are given in Table II.

A. *Experiments of Speed Estimation Stability*

In [22], the unstable speed estimation problem of AFO at low-speed regenerating range is indicated. In this paper, the two robust proposed methods for AFO is designed based on speed estimation stability at all speed range. So it is necessary to verify the feasibility of two proposed methods.

Fig. 25 indicates the experiments of speed estimation stability. Because the unstable region is always at low-speed regenerating range [17], the motor is controlled in regenerating mode and the load is 100% rated load. The reference speed is in sequence of 15, 30, 60, 90, 120 and 150 r/min. In Fig. 25(a) motor runs at low speed regenerating range with zero feedback gains, the estimation is unstable when reference speed is from 60 to 90 r/min with full load. However, the speed estimation is stable with proposed two methods which are shown as Fig. 25(b) and (c). Moreover the estimated speed error is different between Fig. 25(b) and (c).

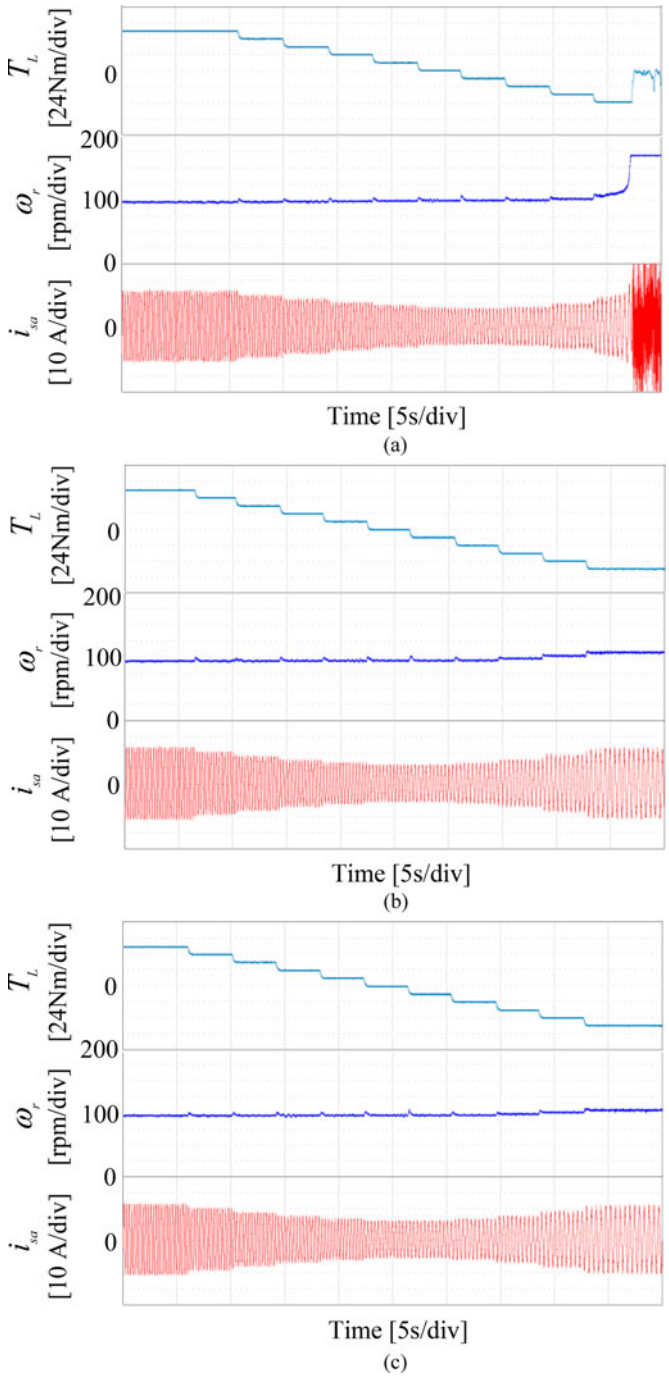

Fig. 26. Stability of speed estimation with variable load torque. (a) Zero feedback gains and classical speed estimation. (b) Robust feedback gains and classical speed estimation. (c) Robust feedback gains and robust speed estimation.

In Fig. 25(b) when the reference speed is 15 r/min, the actual speed is 35 r/min and the estimated speed error is 20 r/min. However the actual speed is 20 r/min and the estimated speed error is 5 r/min in Fig. 25(c). The estimated speed error is

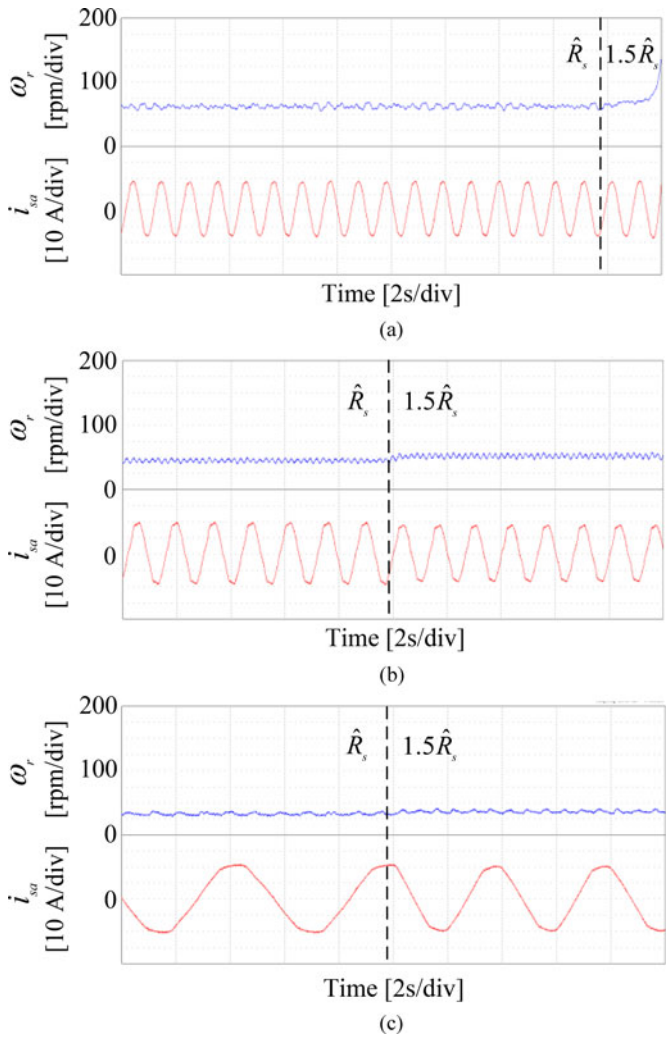

Fig. 27. Robustness to stator resistance deviation at regenerating range, 15 r/min reference speed, 120% rated load. (a) Classical feedback gains and classical speed estimation. (b) Robust feedback gains and classical speed estimation. (c) Robust feedback gains and robust speed estimation.

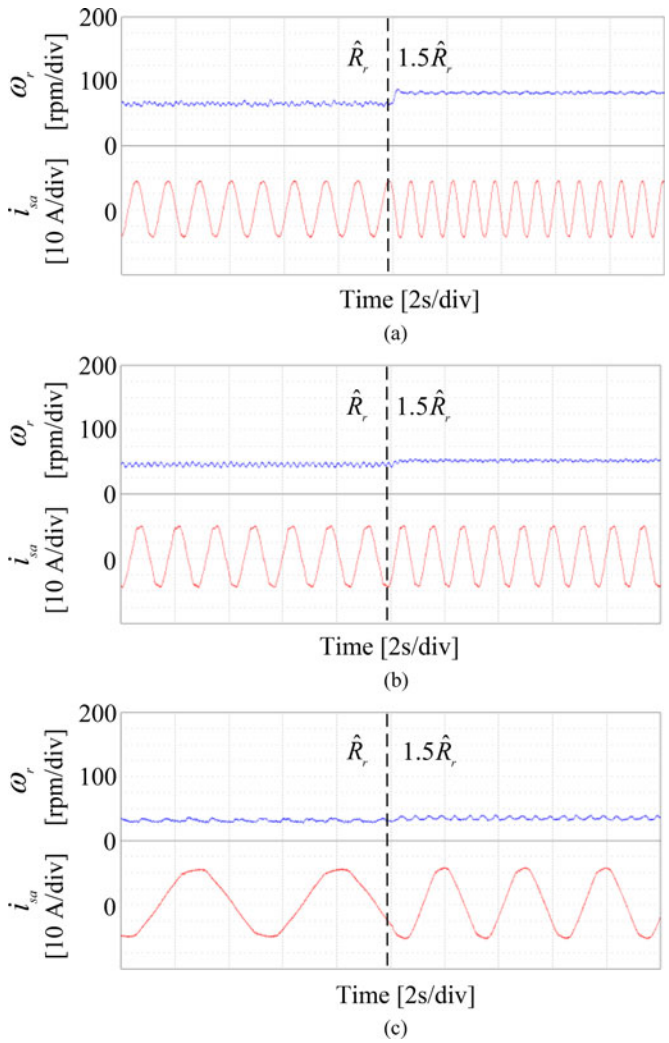

Fig. 28. Robustness to rotor resistance deviation at regenerating range, 15 r/min reference speed, 120% rated load. (a) Classical feedback gains and classical speed estimation. (b) Robust feedback gains and classical speed estimation. (c) Robust feedback gains and robust speed estimation.

mainly caused by parameter deviation and inverter non-linear error [28]–[32]. Inverter nonlinear error is due to:

1) on-state voltage of IGBT;
2) inverter deadtime;
3) delay in turn-on and turn-off process of IGBT.

The speed estimation accuracy is improved further when the robust speed estimation algorithm and the corresponding robust feedback gains are used. The result is as same as the analysis in Section V.

Fig. 26 indicates the experiments that the reference speed is 90 r/min but the load torque is decreased from 120% rated load to –120% rated load. When the load torque is negative the motor is running in regenerating mode. In Fig. 26(a), speed estimation is unstable when the load decreases to –100% rated load. That is mainly because there are some unstable zeros of OLTF when the load is full [22]. However, as indicated in Fig. 26(b) and (c), the stability of speed estimation can be guaranteed at low-speed regenerating range when the two proposed methods are used. It can be seen from Fig. 26(b) and (c), the actual speed is changing from 92 r/min in motoring mode to 102 r/min in regenerating mode when the load varies. That is mainly because the robustness of regenerating mode is weaker than the robustness of motoring mode. Consequently with the same external or internal interrupt, the estimated speed error in regenerating mode is a little bigger than the error in the motoring mode [17].

B. Experiments of Robustness to Motor Parameter Deviation

Fig. 27 indicates the experiment of system robustness to stator resistance deviation. The motor runs in regenerating mode. The reference is 15 r/min and the load is 120% rated load. With CC and when the stator resistance used in AFO increase to 1.5 times, the estimation system is unstable as indicated in Fig. 27(a). That means this method can not endure the 50% stator resistance error with 120% rated load. With CR and 50% stator resistance error, the system can be stable as shown in Fig. 27(b). In the same

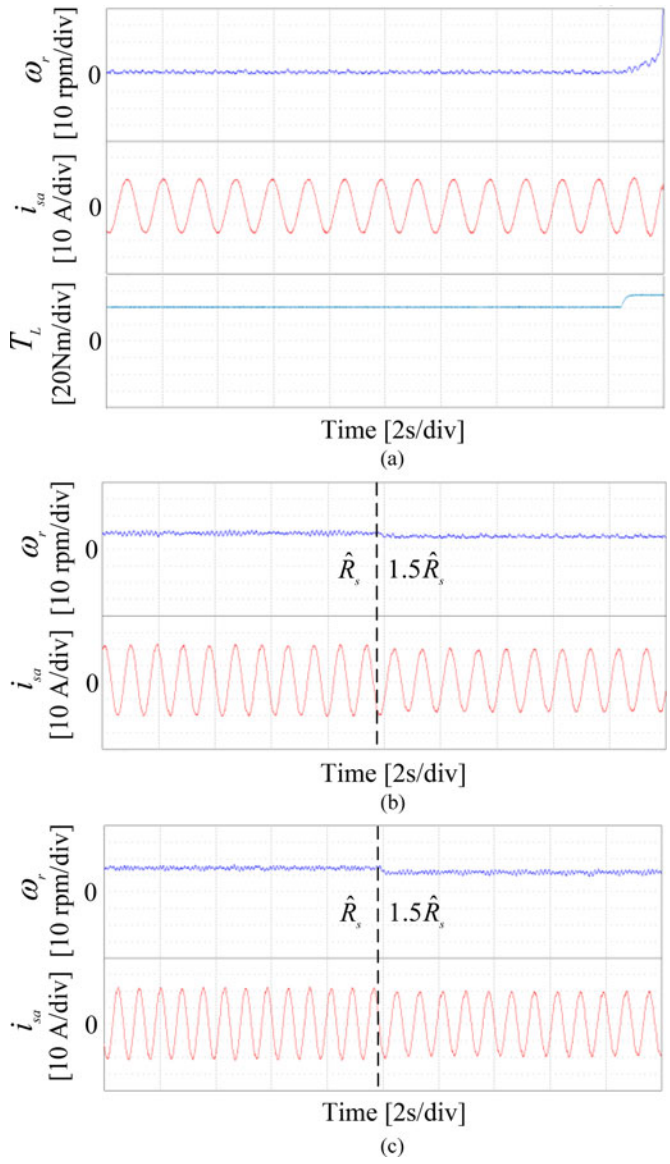

Fig. 29. Robustness to stator resistance deviation at motoring range, 15 r/min reference speed, 120% rated load. (a) Classical feedback gains and classical speed estimation. (b) Robust feedback gains and classical speed estimation. (c) Robust feedback gains and robust speed estimation.

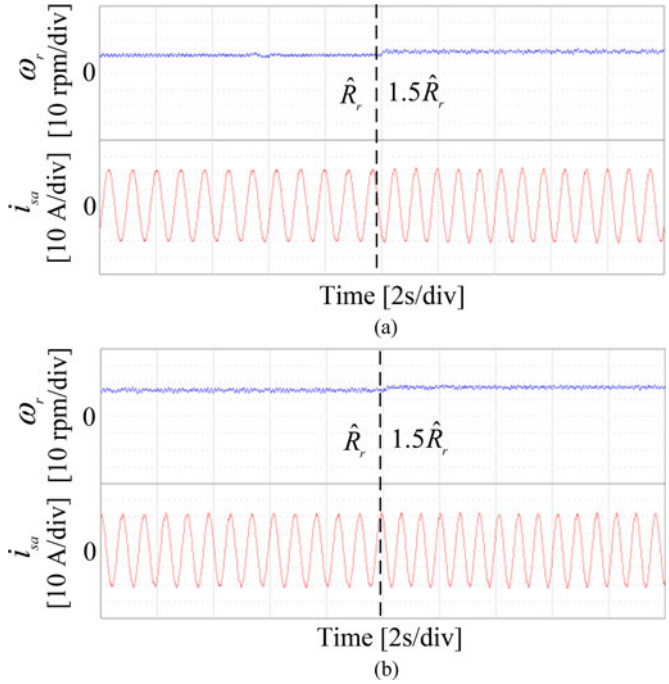

Fig. 30. Robustness to rotor resistance deviation at motoring range, 15 r/min reference speed, 120% rated load. (a) Robust feedback gains and classical speed estimation. (b) Robust feedback gains and robust speed estimation.

way, when RR are used, the system can endure the 50% stator resistance error and keep stable as shown in Fig. 27(c).

Furthermore in Fig. 27 when the stator resistance is accurate, the actual speed is in sequence of 61 r/min with CC, 45 r/min with CR and 30 r/min with RR. When the stator resistance increases by 50%, the actual speed becomes unstable with CC, 55 r/min with CR and 35 r/min with RR. It can be found that compared with CC and CR the speed deviation of RR is smallest even stator resistance is increased by 50%. That means the robustness of RR is the strongest.

Similarly, Fig. 28 indicates the experiment of system robustness to rotor resistance deviation. The motor runs in regenerating mode. The reference is 15 r/min and the load is 120% rated load.

When the rotor resistance is accurate, the actual speed is in sequence of 61 r/min with CC, 45 r/min with CR and 30 r/min with RR. When the rotor resistance increases by 50%, the actual speed becomes 80 r/min with CC, 52 r/min with CR and 35 r/min with RR. The robustness of RR to rotor resistance deviation is the strongest.

Fig. 29 indicates the experiment of system robustness to stator resistance deviation in motoring mode and Fig. 30 is the results to rotor resistance deviation in motoring mode. The reference speed is 15 r/min and the load is 120% rated load.

As shown in Fig. 29(a) based on CC and accurate motor parameters, when the load is 80% rated load, the system can keep stable. However, the actual speed is only 3 r/min. When the load increases to 120% rated load, the system is unstable. That is because the estimated speed error is too large to keep system stable. Compared with CC, the system based on CR or RR can keep stable even when the load is 120% rated load.

In Fig. 29(b) and (c), when the stator resistance is accurate, the actual speed is in sequence of 10 r/min with CR, and 15 r/min with RR. When the stator resistance increases by 50%, the actual speed becomes 6 r/min with CR and 10 r/min with RR. The robustness of RR to stator resistance deviation is still the strongest in motoring mode. Equally it can be seen from Fig. 30 the robustness of RR to rotor resistance deviation is the strongest.

Table IV concludes the estimated speed error in the experiments (from Fig. 25 to 30). The motor operates in regenerating mode with negative load, and in motoring mode with positive load.

C. *Performance at Very Low Speed Range With Huge Load*

Generally when the motor runs at low speed motoring range, the input voltage is small. The inverter nonlinear error and motor parameter deviation have large influence on speed and rotor flux

TABLE IV
ESTIMATED SPEED ERROR IN THE EXPERIMENTS

	Reference Speed	Speed Error with CC	Speed Error with CR	Speed Error with RR
$R_s = \hat{R}_s\, R_r = \hat{R}_r$ −100% load	15 r/min	+20 rpm	+20 r/min	+5 r/min
	30 r/min	+20 r/min	+20 r/min	+9 r/min
	60 r/min	+25 r/min	+15 r/min	+15 r/min
	90 r/min	unstable	+11 r/min	+10 r/min
	120 r/min	unstable	+10 r/min	+10 r/min
	150 r/min	unstable	+10 r/min	+11 r/min
$R_s = 1.5\hat{R}_s$ −120% load	15 r/min	unstable	+40 r/min	+20 r/min
$R_r = 1.5\hat{R}_r$ −120% load		+65 r/min	+37 r/min	+20 r/min
$R_s = 1.5\hat{R}_s$ +120% load		unstable	−9 r/min	−5 r/min
$R_r = 1.5\hat{R}_r$ +120% load		unstable	−3 r/min	+2 r/min

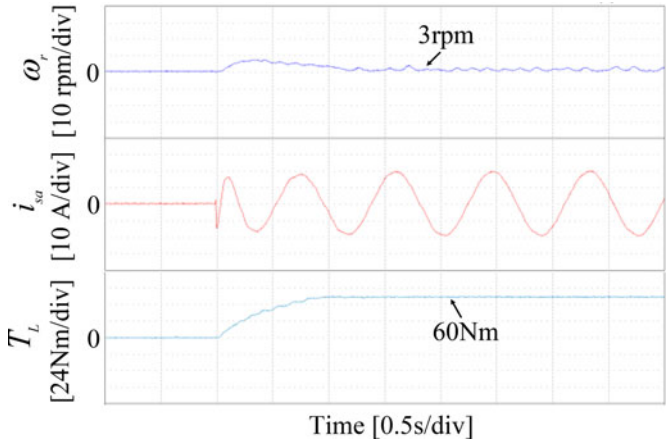

Fig. 31. Starting with 120% rated load, 3 r/min speed reference, robust speed estimation and corresponding robust feedback gains.

estimation. So the motor can not provide huge torque at low speed range as shown in Fig. 29(a). However because of the strong robustness of RR, the accurate estimated speed can be obtained. Consequently the motor can start with 120% rated load and 3 r/min reference speed and run stably as shown in Fig. 31. The performance of proposed method in torque output and speed estimation accuracy is well.

VI. CONCLUSION

In this paper, the different design methods for adaptive full-order observer are divided to two types: 1) without the flux error in the speed estimation and only feedback gains is considered; 2) with the flux error in the speed estimation and combined with feedback gain design. The first type of design method has been researched for many years and there are three typical design methods, but the estimated speed robustness can still be improved. Consequently, a design method, belonging to the first type of design and as the improvement of existed methods, is proposed. Based on stability analysis of speed estimation, there is no stable condition being ignored in the first proposed method. The designed feedback gains can reduce the estimated speed sensitivity to motor parameters especially to the rotor resistance. The second type of design method is the main contribution of this paper. The flux error is introduced into the speed estimation and the closed-loop transfer function of estimated speed is changed. Based on the stability analysis of the speed estimation with flux error, a designed corresponding feedback gains are proposed. With the second proposed method, the stability of observer and speed estimation can be guaranteed. Compared with all the first type of methods, the estimated speed error is reduced much more when the motor parameters are deviated. Especially the estimated speed error is so small that the sensitivity of estimated speed to rotor resistance can be ignored. The two proposed AFO design methods have different advantages and disadvantages. The proposed first method is simple and there are fewer variables in the system than the second method. However, the robustness of the second method is much stronger.

REFERENCES

[1] J. Holtz, "Sensorless control of induction machines—With or without signal injection," *IEEE Trans. Ind. Electron.*, vol. 53, no. 1, pp. 7–30, Feb. 2006.
[2] P. L. Jansen and R. D. Lorenz, "A physically insightful approach to the design and accuracy assessment of flux observers for field oriented induction machine drives," *IEEE Trans. Ind. Appl.*, vol. 30, no. 1, pp. 101–110, Jan./Feb. 1994.
[3] C. Schauder, "Adaptive speed identification for vector control of induction motors without rotational transducers," *IEEE Trans. Ind. Appl.*, vol. 28, no. 5, pp. 1054–1061, Sep./Oct. 1992.
[4] B. Karanayil and M. F. Rahman, "An implementation of a programmable cascaded low pass filter for a rotor flux synthesizer for an induction motor drive," *IEEE Trans. Power Electron.*, vol. 19, no. 2, pp. 253–263, Mar. 2004.
[5] S. Maiti and C. Chakraborty, "Model reference adaptive controller based rotor resistance and speed estimation techniques for vector controlled induction motor drive utilizing reactive power," *IEEE Trans. Ind. Electron.*, vol. 55, no. 2, pp. 594–601, Feb. 2008.
[6] M. Cirrincione and M. Pucci, "An MRAS based sensorless high performance induction motor drive with a predictive adaptive model," *IEEE Trans. Ind. Electron.*, vol. 52, no. 2, pp. 532–551, Apr. 2005.
[7] H. Kubota, K. Matsuse, and T. Nakano, "DSP-based speed adaptive flux observer of induction motor," *IEEE Trans. Ind. Appl.*, vol. 29, no. 2, pp. 344–348, Mar./Apr. 1993.
[8] G. Yang and T. H. Chin, "Adaptive speed identification scheme for a vector controlled speed sensorless inverter induction motor drive," *IEEE Trans. Ind. Appl.*, vol. 29, no. 4, pp. 820–825, Jul./Aug. 1993.
[9] J. Maes and J. Melkebeek, "Speed sensorless direct torque control of induction motors using an adaptive flux observer," *IEEE Trans. Ind. Electron.*, vol. 36, no. 3, pp. 778–785, May/Jun. 2000.
[10] T. Sutikno and N. R. N. Idris, "An improved FPGA implementation of direct torque control for induction machines," *IEEE Trans. Ind. Inform.*, vol. 9, no. 3, pp. 1280–1290, Aug. 2013.
[11] R. Yuan and Z. Q. Zhu, "Direct torque control of permanent-magnet synchronous machine drives with a simple duty ratio regulator," *IEEE Trans. Ind. Electron.*, vol. 61, no. 10, pp. 5249–5258, Oct. 2014.
[12] X. Wei and R. D. Lorenz, "Dynamic loss minimization using improved deadbeat-direct torque and flux control for interior permanent-magnet synchronous machines," *IEEE Trans. Ind. Appl.*, vol. 50, no. 2, pp. 1053–1065, Mar./Apr. 2014.
[13] A. Davari and D. A. Khaburi, "Using full order and reduced order observers for robust sensorless predictive torque control of induction motors," *IEEE Trans. Power Electron.*, vol. 27, no. 7, pp. 3424–3433, Jul. 2012.
[14] M. Hinkkanen and L. Harnefors, "Reduced-order flux observers with stator-resistance adaptation for speed-sensorless induction motor drives," *IEEE Trans. Power Electron.*, vol. 25, no. 5, pp. 1173–1183, May 2010.
[15] A. Francesco, D. Filippo, and A. Sferlazza, "Sensorless control of induction motor drive based on robust Kalman filter and adaptive speed

estimation," *IEEE Trans. Ind. Electron.*, vol. 61, no. 3, pp. 1444–1453, Mar. 2014.
[16] K. Wang and B. Chen, "Online updating of rotor time constant based on combined voltage and current mode flux observer for speed-sensorless AC drives," *IEEE Trans. Ind. Electron.*, vol. 61, no. 9, pp. 4583–4593, Sep. 2014.
[17] K. Ohyama and G. M. Asher, "Comparative analysis of experimental performance and stability of sensorless induction motor drives," *IEEE Trans. Ind. Electron.*, vol. 53, no. 1, pp. 178–186, Feb. 2006.
[18] M. Marchesoni, P. Segarich, and E. Soressi, "A simple approach to flux and speed observation in induction motor drives," *IEEE Trans. Ind. Electron.*, vol. 44, no. 4, pp. 528–535, Aug. 1997.
[19] M. Hasegawa and S. Furutani, "Robust vector control of induction motors using full-order observer in consideration of core loss," *IEEE Trans. Ind. Electron.*, vol. 50, no. 5, pp. 912–919, Oct. 2003.
[20] H. Lennart and M. Hinkkanen, "Complete stability of reduced-order and full-order observers for sensorless IM drives," *IEEE Trans. Ind. Electron.*, vol. 55, no. 3, pp. 1319–1329, Mar. 2008.
[21] M. Hinkkanen and J. Luomi, "Parameter sensitivity of full-order flux observers for induction motors," *IEEE Trans. Ind. Appl.*, vol. 39, no. 4, pp. 1127–1135, Jul./Aug. 2003.
[22] S. Suwankawin and S. Sangwongwanich, "Design strategy of an adaptive full-order observer for speed-sensorless induction-motor drives-tracking performance and stabilization," *IEEE Trans. Ind. Electron.*, vol. 53, no. 1, pp. 96–119, Feb. 2006.
[23] T. Tuovinen and M. Hinkkanen, "Adaptive full-order observer with high-frequency signal injection for synchronous reluctance motor drives," *IEEE J. Emerging Sel. Topics Power Electron.*, vol. 2, no. 2, pp. 181–189, Jun. 2014.
[24] P. Vaclavek and P. Blaha, "AC drive observability analysis," *IEEE Trans. Ind. Electron.*, vol. 60, no. 8, pp. 3047–3059, Aug. 2013.
[25] S. Po-ngam and S. Sangwongwanich, "Stability and dynamic performance improvement of adaptive full-order observers for sensorless PMSM drive," *IEEE Trans. Power Electron.*, vol. 27, no. 2, pp. 588–600, Feb. 2012.
[26] T. Tuovinen and M. Hinkkanen, "Comparison of a reduced-order observer and a full-order observer for sensorless synchronous motor drives," *IEEE Trans. Ind. Appl.*, vol. 48, no. 6, pp. 1959–1967, Nov./Dec. 2012.
[27] W. Chen, "Low speed stability research of adaptive full-order observer for induction motor," in *Proc. Chin. Soc. Electr. Eng.*, 2010, pp. 33–40.
[28] N. Urasaki and T. Senjyu, "An adaptive dead-time compensation strategy for voltage source inverter fed motor drives," *IEEE Trans. Power Electron.*, vol. 20, no. 5, pp. 1150–1160, Sep. 2005.
[29] M. Tsuji and S. Chen, "A sensorless vector control system for induction motors using q-axis flux with stator resistance identification," *IEEE Trans. Ind. Electron.*, vol. 48, no. 1, pp. 185–194, Feb. 2001.
[30] C. Jong-Woo and S. Sul, "A new compensation strategy reducing voltage/current distortion in PWM VSI systems operating with low output voltages," *IEEE Trans. Ind. Appl.*, vol. 31, no. 5, pp. 1001–1008, Sep./Oct. 1995.
[31] G. Pellegrino and R. I. Bojoi, "Accurate inverter error compensation and related self-commissioning scheme in sensorless induction motor drives," *IEEE Trans. Ind. Appl.*, vol. 46, no. 5, pp. 1970–1978, Sep./Oct. 2010.
[32] G. Pellegrino and R. I. Bojoi, "Self-commissioning algorithm for inverter nonlinearity compensation in sensorless induction motor drives," *IEEE Trans. Ind. Appl.*, vol. 46, no. 4, pp. 1416–1424, Jul./Aug. 2010.
[33] V. R. Jevremovic and V. Vasic, "Speed-sensorless control of induction motor based on reactive power with rotor time constant identification," *IET Electr. Power Appl.*, vol. 4, no. 6, pp. 462–473, Jul. 2010.
[34] Z. Yin, C. Zhao, J. Liu, and Y. Zhong, "Research on anti-error performance of speed and flux estimator for induction motor using robust reduced-order EKF," *IEEE Trans. Ind. Inform.*, vol. 9, no. 2, pp. 1037–1046, May 2013.

Wei Sun received the B.S. degree in electrical engineering from Beijing Jiaotong University, Beijing, China, in 2009, and the M.S. degree in electrical engineering from the Harbin Institute of Technology, Harbin, China, in 2012. He is currently working toward the Ph.D. degree at the School of Electrical Engineer and Automation, Harbin Institute of Technology.

His main field of interest is induction motor and permanent magnet motor drive, control theory application in electrical drives and robustness improvement of industry application.

Yong Yu was born in China in 1974. He received the B.S. degree in electromagnetic measurement and instrumentation from the Harbin Institute of Technology (HIT), Harbin, China, and the M.S. and Ph.D. degrees in electrical engineering from HIT, in 1997 and 2003, respectively.

Since 2004, he has been an Associate Professor at HIT. His current research interests include electrical motor drives, power quality mitigation, and fault diagnosis and tolerant control of inverter.

Gaolin Wang (M'13) received the B.S., M.S. and Ph.D. degrees in electrical engineering from the Harbin Institute of Technology, Harbin, China, in 2002, 2004, and 2008, respectively.

In 2009, he joined the Department of Electrical Engineering, Harbin Institute of Technology, as a Lecturer, where he has been a Professor of electrical engineering since 2014. From 2009 to 2012, he was a Postdoctoral Fellow at Shanghai STEP Electric Corporation. He has authored more than 30 technical papers published in journals and conference proceedings. He is the holder of seven Chinese patents. His current major research interests include permanent magnet synchronous motor drives, high performance direct-drive for traction system, position sensorless control of ac motors and efficiency optimization control of interior PMSM.

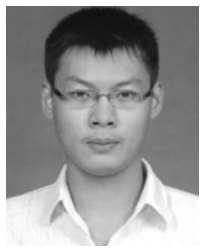

Binbin Li was born in 1989. He received the B.S. and M.S. degrees in electrical engineering from the Harbin Institute of Technology, Harbin, China, in 2010 and 2012, respectively, where he is currently working toward the Ph.D. degree.

His research interests include high-power electronics, multilevel converters, control algorithms, and PWM techniques.

Dianguo Xu (M'97–SM'12) received the B.S. degree in control engineering from the Harbin Engineering University, Harbin, China, in 1982, and the M.S. and Ph.D. degrees in electrical engineering from the Harbin Institute of Technology (HIT), Harbin, in 1984 and 1989, respectively.

In 1984, he joined the Department of Electrical Engineering, HIT, as an Assistant Professor. Since 1994, he has been a Professor at the Department of Electrical Engineering, HIT. He was the Dean of the School of Electrical Engineering and Automation, HIT, from 2000 to 2010. He is currently the Vice President of HIT. His research interests include renewable energy generation technology, power quality mitigation, sensorless vector controlled motor drives, high performance PMSM servo system. He has published more than 600 technical papers. He is an Associate Editor of the IEEE TRANSACTIONS ON INDUSTRIAL ELECTRONICS and the IEEE JOURNAL OF EMERGING AND SELECTED TOPICS IN POWER ELECTRONICS. He serves as the Chairman of IEEE Harbin Section.